How CD4+ T-cell help shapes functional and dysfunctional CD8+ T-cell differentiation

Busselaar, J.L.C.

Chapter 5

Requirements for development of T-helper1 and T-follicular helper cells from a common precursor

Douwe M. T. Bosma[1,2*], Julia Busselaar[1,2*], Mo D. Staal[1,2**], Mylene de Koning[1**], Mirna Reljić[1], Xin Lei[1,2], Tom de Wit[1,2], Yanling Xiao[1,2], Jannie Borst[1,2,3***] and Fiamma Salerno[1***]

[1]Department of Immunology;

[2]Oncode Institute, Leiden University Medical Center, 2333 ZA Leiden, The Netherlands

*Shared first authors;

**Shared second authors;

***Shared last authors

Cell Reports 2026; 45(5): 117296

DOI: 10.1016/j.celrep.2026.117296

Abstract

T-helper1 (Th1) and T-follicular helper (Tfh) cells support cellular and humoral immunity, respectively. How activated $CD4^+$ T cells commit to these fates remains unclear. Using a mouse vaccination model, we traced endogenous, polyclonal $CD4^+$ T cells during bifurcation into Th1 and Tfh lineages. We found that Th1 and Tfh cells originate from shared, highly proliferative $TCF1^+SLAMF6^+PD\text{-}1^+$ precursor clones that co-express Th1- and Tfh-related transcription factors and chemokine receptors, including T-bet, BCL6, CXCR3 and CXCR5. Generation of common Th1/Tfh precursors from naive $CD4^+$ T cells requires CD28 costimulation, but occurs independently of CD40, ICOS, and interaction with type-1 conventional dendritic cells (cDC1s) or B cells. Lineage commitment subsequently diverges: differentiation into Th1 cells relies on CD40 costimulation and cDC1s, whereas differentiation into Tfh cells requires ICOS costimulation and B cells. Activated $CD4^+$ T cells thus give rise to a common Th1/Tfh precursor whose fate depends on interactions with distinct antigen-presenting cells.

Introduction

Upon antigen encounter within secondary lymphoid organs, CD4$^+$ T cells are activated, clonally expand and initiate differentiation into T-helper (Th)1, 2 or 17 lineages to regulate cellular immunity[1]. At the same time, T-follicular helper (Tfh) cells are formed, which promote B-cell expansion and differentiation in germinal centers (GC)[2]. During a type-I immune response, Th1 and Tfh cells emerge in parallel, suggesting a bifurcation in their effector differentiation trajectories[3-5]. Tfh cells are likewise generated in parallel with Th2 or Th17 effector CD4$^+$ T cells[6,7] and acquire pathogen-tailored functional diversity[8]. Coordination of cell-mediated and humoral immunity thus depends on Th/Tfh lineage decision making in activated CD4$^+$ T cells. This process is a potential target for therapeutic intervention e.g. in vaccination, cancer and auto-immunity.

Effector CD4$^+$ T-cell differentiation relies on successive interactions with different professional antigen-presenting cells (APCs) and is initiated upon cognate contact with conventional dendritic cells (cDCs). Among these, the cDC2 lineage excels at (soluble) antigen presentation in major histocompatibility complex (MHC)-II molecules[9] and is important for initial CD4$^+$ T-cell activation[10,11]. The cDC1 lineage is much more proficient in phagocytosing cell-bound antigen and cross-presenting this in MHC-I molecules, thus playing a crucial role in CD8$^+$ T-cell activation[12-14]. cDC1s can also contribute to CD4$^+$ T-cell priming[15,16] and relay help for effector and memory differentiation of CD8$^+$ T cells[17,18]. In contrast, B cells are considered essential APCs to promote CD4$^+$ T-cell differentiation into Tfh cells[4,19].

In general, effector differentiation of CD4$^+$ T cells is guided by the activation and maturation state of cDCs and B cells, which are reflected in their costimulatory and cytokine profiles[1,7,10]. These inputs, as delivered during multiple sequential interactions between T cells and APCs, collectively regulate expression of lineage-determining transcription factors that direct Th differentiation along specific trajectories. Decision-making between Th and Tfh lineage commitment likewise depends on specific transcription factors. Whereas transient co-expression of T-bet and BCL6 has been reported in *in vitro* T-cell cultures[20], *in vivo* studies indicate that the choice between Th1 and Tfh cell differentiation depends on the ratio of T-bet versus BCL6 protein levels, which is determined by initiation of negative regulatory circuits. For example, BCL6 represses genes encoding Th1, Th2 and Th17 lineage-specific transcription factors, including *Tbx21* (encoding T-bet), *Gata3* and *Rora*[21,22]. However, when it binds to T-bet, BCL6 can no longer repress the *Prdm1* gene encoding BLIMP1. As a result, BLIMP1 starts to suppress Tfh-associated genes, thus favoring Th1 differentiation[23,24]. In contrast, transient early T-bet expression is required for upregulation of CXCR5 and generation of IFNγ-producing Tfh cells in response to infection[25,26].

CD4$^+$ T-cell differentiation to either Th1 or Tfh cell fate has largely been studied as separate processes[3], rather than interrogating how these parallel outcomes emerge within the same immune response. Also, much of our current understanding derives from experimental systems

based on T-cell receptor (TCR) transgenic CD4$^+$ T cells[4,27-29], leaving open the question of how Th1 and Tfh differentiation unfolds within endogenous, polyclonal CD4$^+$ T-cell populations. This is a relevant distinction, since TCR affinity has been proposed to impact CD4$^+$ T-cell fate decisions in some studies[28-30], but not in others[10,27], highlighting the need to examine differentiation dynamics in polyclonal contexts. In addition, deconvolution of CD4$^+$ T-cell differentiation trajectories *in vivo* can be challenged by the high plasticity of T-helper lineages[31,32] and stochastic events[33]. As a result, the temporal and mechanistic relationships between early activation states and downstream Th1 or Tfh commitment remain poorly defined in intact immune responses. Addressing these gaps is essential for understanding how immune responses are tailored toward cellular or humoral immunity and for identifying stages at which CD4$^+$ T-cell fate might be therapeutically redirected.

In this study, we used a vaccination-based mouse model to induce and longitudinally trace Th1 and Tfh cell differentiation from endogenous, polyclonal CD4$^+$ T cells. By integrating high-dimensional flow cytometry with single-cell RNA-sequencing (scRNAseq) and TCR-sequencing, we show that antigen-specific CD4$^+$ T clones pass through a common Th1/Tfh precursor state, before committing to a specific differentiation trajectory. We define the gene and protein expression profile of this precursor, demonstrate its presence across different infectious contexts in mice, and identify key costimulatory signals and antigen-presenting cell interactions that guide its formation and commitment toward either the Th1 or Tfh lineage. Together, these findings provide mechanistic insight into how CD4$^+$ T-cell fate decisions are regulated in physiologically relevant, polyclonal immune responses.

Results

Vaccination raises endogenous, functional Th1 and Tfh cells in equal measure

To study how endogenous, polyclonal CD4$^+$ T cells differentiate *in vivo*, we used a mouse vaccination model that has previously revealed the effects of CD4$^+$ T-cell help on effector and memory CD8$^+$ T-cell differentiation[34-36]. In this model, we vaccinate C57BL/6 mice with plasmid DNA encoding an immunodominant MHC-I (H-2D^b) restricted epitope $E7_{48-57}$ from human papilloma virus (HPV) either alone (Control) or linked to three MHC-II-restricted helper epitopes: p30, PADRE, and NEF (MHC-II) (Figure 1A). These MHC-II-restricted epitopes were selected for binding to human HLA-DP, -DQ and -DR, respectively[37], but p30 and PADRE can also be presented by MHC-II (I-A^b)[38,39] and prime CD4$^+$ T-cell responses in mice[34,40]. The plasmid DNA vaccine is "tattooed" on days 0, 3 and 6 into the depilated skin of the hind leg and expressed in keratinocytes, followed by antigen delivery to the draining lymph node (dLN) by cDCs and by passive drainage[41,42]. The antigen-specific CD4$^+$ T-cell response can be followed by flow cytometry using an MHC-II tetramer (tet) against the PADRE epitope (Figure 1B). PADRE tet$^+$ CD4$^+$ T cells were detected in the dLN from day 4 onwards after vaccination (Figure 1C)

and entered the circulation by day 5 (Figure S1A). In line with a type-1 immune response raised by this model, CD44$^+$ PADRE tet$^+$ cells differentiated into Th1 and Tfh cells, but not into T-regulatory (Treg), Th2 or Th17 cells (Figure S1B). PADRE tet$^+$ cells were divided into cells that retain PSGL1 (PSGL1$^+$ CXCR5$^-$) or cells that lose PSGL1 but acquire CXCR5 (PSGL1$^-$ CXCR5$^+$) (Figure 1D). Within the PSGL1$^+$ CXCR5$^-$ cell population, Th1 cells were defined as SLAM$^+$ T-bet$^+$ BCL6$^-$ PD-1^{low} FR4^{low} TCF1^{low} (Figure 1D, Figure S1C)[43-45]. Within the PSGL1$^-$ CXCR5$^+$ cell population, Tfh cells were defined as SLAM$^-$ T-bet$^-$ BCL6$^+$ PD-1^{hi} FR4$^+$ TCF1^{hi} (Figure 1D, Figure S1C)[3,7,43,46]. Th1 and Tfh populations emerged in parallel and were of similar size at day 4 after vaccination (Figure 1E). By day 5, when PADRE tet$^+$ CD4$^+$ T cells became detectable in the blood (Figure S1A), Tfh cells started accumulating in the dLN (Figure 1E). At that day, Th1 cells went from the dLN to the blood, where they represented ~50% of PADRE$^+$ CD4$^+$ T cells (Figure 1F).

To validate the helper functions of Th1 and Tfh cells, we investigated the CD8$^+$ T-cell and B-cell responses post vaccination. Mice in which CD4$^+$ T cells were activated by the MHC-II vaccine displayed an increased frequency of KLRG1$^+$ effector phenotype E7 tet$^+$ CD8$^+$ T cells at day 10 in the blood compared to mice receiving the control vaccine (Figure 1G; Figure S1D). These data confirm that Th1 cells generated by the MHC-II vaccine contributed to effector differentiation of CD8$^+$ T cells raised by the E7 epitope, as demonstrated before[34,36]. Mice that received the MHC-II vaccine also displayed increased frequencies of CD19$^+$ IgD$^-$ CD38$^-$ FAS$^+$ GL7$^+$ germinal center (GC) B cells and CD138$^+$ TACI$^+$ plasmablasts (Figure 1H; Figure S1E, F), confirming that vaccine-primed Tfh cells promoted the B-cell response. Thus, both Th1 and Tfh cells raised by the MHC-II vaccine are functionally competent. Inhibition of T-cell egress from the dLN with sphingosine 1-phosphate (S1P) receptor-targeting drug FTY720 increased the overall frequency of PADRE tet$^+$ CD4$^+$ T cells in the dLN by more than 2-fold (Figure S1G, H). At day 7 after vaccination, PADRE tet$^+$ Th1 and Tfh cell frequencies and absolute numbers were comparable in dLN of FTY720-treated mice (Figure 1I; Figure S1I). This finding indicates that the MHC-II vaccine leads in equal measure to Th1 and Tfh differentiation, making it a good model for studying the differentiation trajectories of the endogenous vaccine-specific CD4$^+$ T cells.

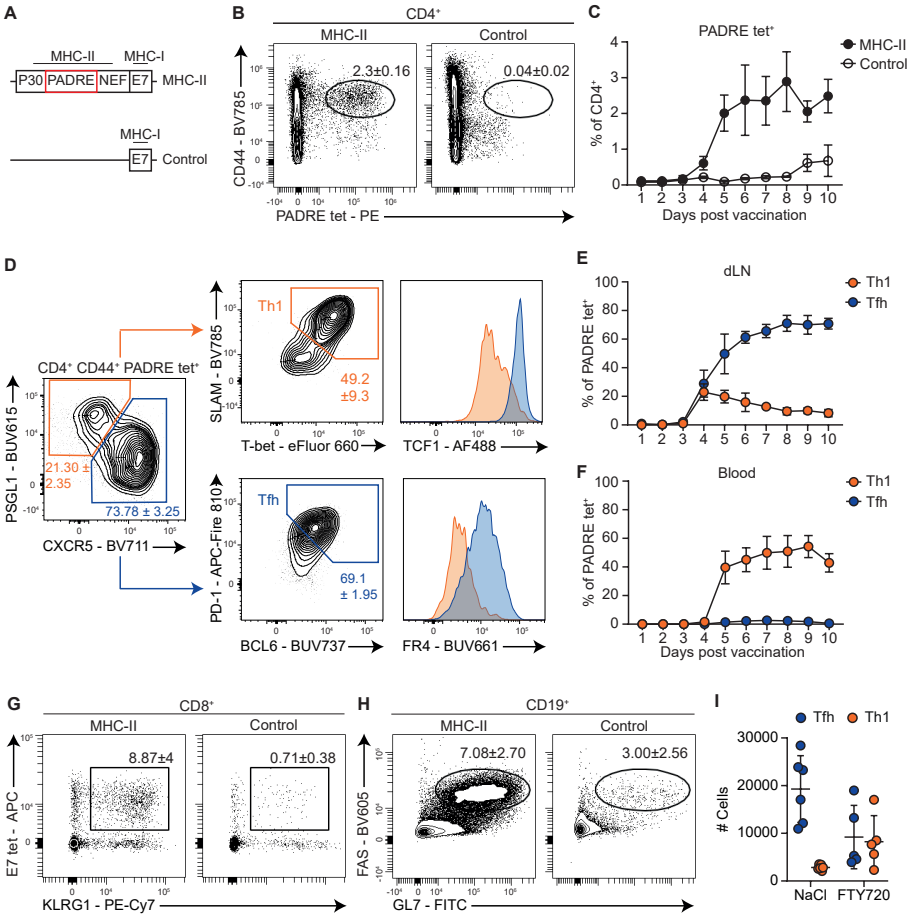

Figure 1. A vaccination model to study differentiation of endogenous, polyclonal CD4⁺ T cells into Th1 or Tfh cells. (A) Scheme of epitopes in MHC-II and control DNA vaccines. (B) Representative flow cytometry plots depicting frequency of CD44⁺ PADRE tet⁺ CD4⁺ T cells in dLN at day 5 post-vaccination (N=3, mean ± SD). (C) Frequency of PADRE tet⁺ CD4⁺ T cells in dLN over time (N=8 for MHC-II, N=3 for Control). (D) Representative flow cytometry plots depicting the phenotype of CD44⁺ PADRE tet⁺ CD4⁺ T cells in the dLN at day 8 post-vaccination, and identifying Th1 cells (orange) as PSGL1^{hi} CXCR5^{-} SLAM⁺ T-bet⁺ FR4^{low} TCF1^{low} and Tfh cells (blue) as PSGL1$^{int-low}$ CXCR5⁺ BCL6⁺ PD-1^{hi} FR4^{hi} TCF1^{hi}. (E, F) Frequency of Tfh (CXCR5⁺ PSGL1^{lo} PD-1⁺ BCL6⁺) and Th1 cells (CXCR5^{-} PSGL1^{hi} T-bet⁺ SLAM⁺) within PADRE tet⁺ CD4⁺ T cells in dLN (E) or blood (F) over time after MHC-II-vaccination (N=5). (G) Representative contour plots depicting antigen-specific effector CD8⁺ T cells (E7 tet⁺ KLRG1⁺) in blood at day 10 after MHC-II or control vaccination. (H) Representative contour plots depicting CD19⁺ IgD^{-} CD38^{-} FAS⁺ GL7⁺ GC B cells in the dLN at day 8 after MHC-II or control vaccination. (I) Absolute numbers of Th1 and Tfh PADRE tet⁺ CD4⁺ T cells in dLN at day 7 post-vaccination (N=6 mean ± SD).

Reconstruction of the Th1- and Tfh differentiation trajectories that evolve after vaccination

To gain insight into the temporal changes that $CD4^+$ T cells undergo during Th1 and Tfh differentiation, we analyzed PADRE tet^+ $CD4^+$ T cells in the dLNs of mice from day 4 to 9 after vaccination by spectral flow cytometry and dimension reduction analysis (Figure 2A; Figure S2A). To ensure that we captured the full differentiation trajectory, we gated on total $CD4^+$ PADRE tet^+ cells, which include a small proportion of $CD62L^{hi}$ $CD44^{low}$ naive cells. Indeed, PADRE tet^+ $CD4^+$ T cells were discriminated into naive $CD62L^{hi}$ $CD44^{low}$ and activated $CD44^{hi}$ cells (Figure 2B). The marker profile of the activated $PADRE^+$ $CD4^+$ T-cell pool underwent daily remodeling and displayed progressive branching towards two end points (Figure 2A; Figure S2A), which were characterized by a Th1 ($PSGL1^+$ T-bet^+ $SLAM^+$ $TCF1^-$ $SLAMF6^-$) or a Tfh ($CXCR5^+$ $PD\text{-}1^+$ $BCL6^+$ $TCF1^+$ $SLAMF6^+$ $FR4^+$) phenotype (Figure 2C-E), as we had observed before (Figure 1D, Figure S1C).

To reconstruct the temporal evolution of PADRE tet^+ $CD4^+$ T-cell differentiation towards Th1 and Tfh states, we used Wishbone, an algorithm that orders cells according to their developmental progression and infers branching trajectories into only one of two possible fates[47]. Wishbone calculates differentiation trajectories based on the rise and fall of phenotypic markers and uses nearest-neighbor graphs to capture developmental distance from a starting point, which we defined as the $CD62L^{hi}$ $CD44^{low}$ naive $CD4^+$ T-cell state. In our experimental setup, PADRE tet^+ $CD4^+$ T cells were ordered based on early activation (CD44, CD62L) and stem-like markers (TCF1, SLAMF6), as well as acquisition of the Th1 or Tfh phenotype (PSGL1, T-bet, SLAM, CXCR5, PD-1, BCL6 and FR4). PADRE tet^+ $CD4^+$ T cells were positioned along either the trunk or one of the two possible branches of the trajectory (Figure 2F; Figure S2B). Wishbone identified $PSGL1^+$ T-bet^+ $SLAM^+$ Th1 cells as branch 1 and $CXCR5^+$ $PD\text{-}1^+$ $BCL6^+$ $TCF1^+$ $FR4^+$ Tfh cells as branch 2 (Figure 2C-F). In contrast, the trunk of the Wishbone trajectory was composed of $CD62L^{hi}$ $CD44^{low}$ naive cells and $CD62L^{hi}$ $CD44^{hi}$ activated cells (Figure 2B, F). The $CD44^{hi}$ $CD62L^{hi}$ cells expressed high levels of TCF1 and SLAMF6 (Figure 2C), which are considered markers of stem-like $CD4^+$ T cells[45,48,49], thus suggesting the potential of $CD44^{hi}$ $CD62L^{hi}$ cells for further differentiation. In addition, $CD44^{hi}$ $CD62L^{hi}$ cells in the trunk of the trajectory had higher levels of CXCR5, BCL6 and PD-1 compared to naive cells, but still expressed PSGL1 (Figure 2D, E). Apart from being highly expressed by Tfh cells, PD-1 is also upregulated as a result of TCR triggering[50,51], and in line with this, all $CD44^{hi}$ cells had higher expression of PD-1 compared to $CD62L^{hi}$ $CD44^{low}$ naive cells (Figure 2E). We also show that the pseudotime calculated by Wishbone matched real-time differentiation, as visualized by the decrease in frequency of $CD62L^{hi}$ $CD44^{low}$ and $CD62L^{hi}$ $CD44^{hi}$ cells over time (Figure S2A, C). Altogether, these data suggest that, upon activation, antigen-specific $CD4^+$ T cells pass through a common $TCF1^+$ $SLAMF6^+$ $PD\text{-}1^+$ $CXCR5^+$ $BCL6^+$ $PSGL1^+$ cell state before branching into Th1 or Tfh differentiation states.

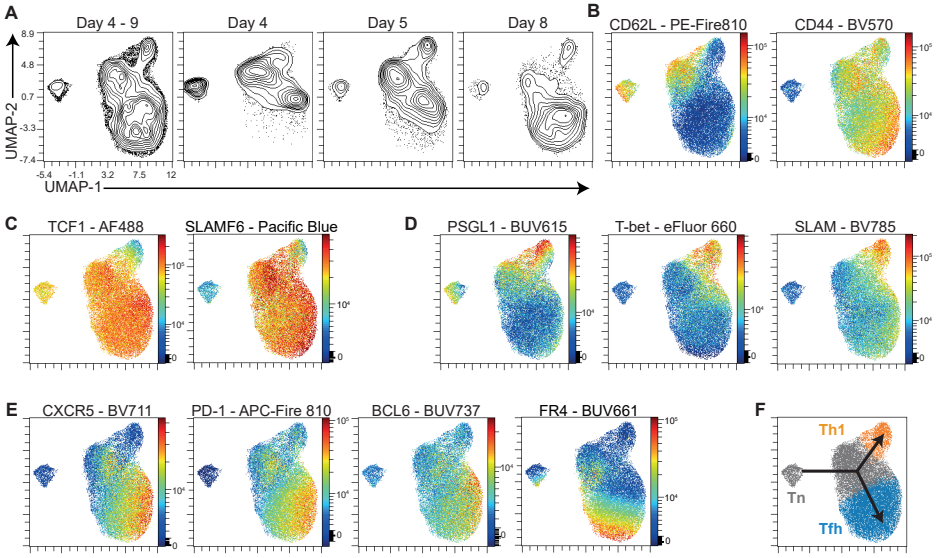

Figure 2. Temporal analysis highlights a common differentiation branchpoint for Th1 and Tfh cells. (A) UMAP projections showing concatenated PADRE tet$^+$ CD4$^+$ T cells in dLN from day 4-9 post-vaccination, or single projections at days 4, 5 or 8 (N=5 per time point). (B-E) Overlay of CD62L and CD44 (B), TCF1 and SLAMF6 (C), PSGL1, T-bet and SLAM (D) and CXCR5, PD-1, BCL6 and FR4 expression (E). (F) Overlay of Wishbone branching on UMAP from panel D. Arrows depict differentiation branches. Grey: trunk; orange: branch 1, identified as Th1 cells; blue: branch 2, identified as Tfh cells.

Th1 and Tfh cells develop from common precursor clones according to single-cell TCR sequencing

To characterize CD4$^+$ T-cell differentiation trajectories in an unbiased manner, we performed scRNAseq and paired TCRseq on activated CD3$^+$ CD44^{hi} T cells that were flow cytometrically purified from the dLN of mice at days 5 and 10 post-vaccination (Figure S3A). The MHC-II vaccine contains multiple CD4$^+$ T-cell epitopes[34], while only the responders to PADRE are detectable by MHC-II tetramer staining. We therefore analyzed the total activated T-cell population to capture the full spectrum of responding endogenous T cells, rather than restricting the analysis to a single antigen specificity. Consistent with this design, PADRE tet$^+$ cells comprised approximately 10% and 19% of the total CD44^{hi} effector population at days 5 and 10 post-vaccination, respectively (Figure S3B). After quality control filtering, selection of cells co-expressing TCRα and TCRβ sequences and exclusion of CD8$^+$ T cells and γδ T cells (Figure S3C), we obtained 4656 CD4$^+$ T cells for data analysis. Dimensionality reduction and clustering of cells based on their gene expression profiles identified 7 clusters that contained more than 20 cells (Figure 3A, B; Figure S3D, Table S1). Clusters 0 and 4 identified two Treg cell populations, characterized by expression of *Foxp3*, *Ctla4* and *Il2ra* (encoding CD25) (Figure 3C). Cluster 1 identified Tfh cells expressing *Tcf7* (encoding TCF1), *Cxcr5*, *Bcl6* and *Pdcd1* (encoding PD-1); cluster 2 identified

Th1 cells expressing *Selplg* (encoding PSGL1), *Tbx21* (encoding T-bet), *Id2*, and *Cxcr3*; cluster 3 identified naive-like cells expressing *Ccr7*, *Lef1*, *Sell* (encoding CD62L), and *Tcf7*; whereas cluster 6 was dominated by an interferon (IFN)-stimulated gene (ISG) signature (Figure 3C). Interestingly, cluster 5 contained cells expressing both Th1-related genes (*Tbx21*, *Cxcr3*) and Tfh-related genes (*Tcf7*, *Cxcr5*, *Bcl6*, *Pdcd1*) (Figure 3C), supporting the existence of a common Th1/Tfh precursor. The expression levels of these genes were intermediate between those found in Th1 cells (cl. 2) and Tfh cells (cl. 1). Cells of cluster 5 also expressed *Pdcd1* and *Cd69*, which are markers of recent TCR triggering (Figure 3C)[50-53], and were higher in frequency at day 5 after vaccination than at day 10, supporting that they represent recently activated cells (Figure 3B). The frequency of Th1 cells (cl. 2) and Tfh cells (cl. 1) on the other hand, increased over time (Figure 3B), which aligns with ongoing effector differentiation of the activated $CD4^+$ T-cell pool.

Next, to define clonal relationships between responder $CD4^+$ T cells in different states of effector differentiation, we paired the gene expression profiles per cell with TCRα and TCRβ sequence information. TCR clones were defined based on identical TCRα and TCRβ complementarity region (CDR)3 sequences, which identified a total number of 3549 clones within the $CD4^+$ T-cell compartment. We noted that Tfh cluster 1, Th1 cluster 2 and the intermediate phenotype cluster 5 had the highest frequency of expanded clones (>1 cell per clone) among all clusters (Figure 3D). Additionally, the highest number of expanded clones was observed in Tfh cluster 1, followed by Th1 cluster 2, intermediate phenotype cluster 5 and Treg cluster 0 (Figure S3E, F). Out of 352 expanded clones, 171 clones were shared between two or more clusters, while the rest was uniquely expanded within one cluster (Figure S3E). Tregs of cluster 0 comprised more unique than shared clones and sharing occurred primarily with Tregs of cluster 4 (Figure 3E, Figure S3F). The majority (72%) of expanded clones was shared between Tfh and Th1 cells (cl. 1 and 2), Tfh or Th1 cells and intermediate phenotype cells (cl. 5), or all three populations (Figure 3E), which was evident at both day 5 and day 10 after vaccination (Figure 3F). These data thus demonstrate the clonal relationship between cluster 5 cells and Th1 and Tfh cells and validate the indication from flow cytometry and associated Wishbone analysis (Figure 2) that antigen-activated $CD4^+$ T cells go through a common precursor state expressing both Th1 and Tfh-related genes, from which they can further develop into committed Th1 or Tfh cells. Cluster 5 cells thus represent the common precursors of Th1 and Tfh lineages.

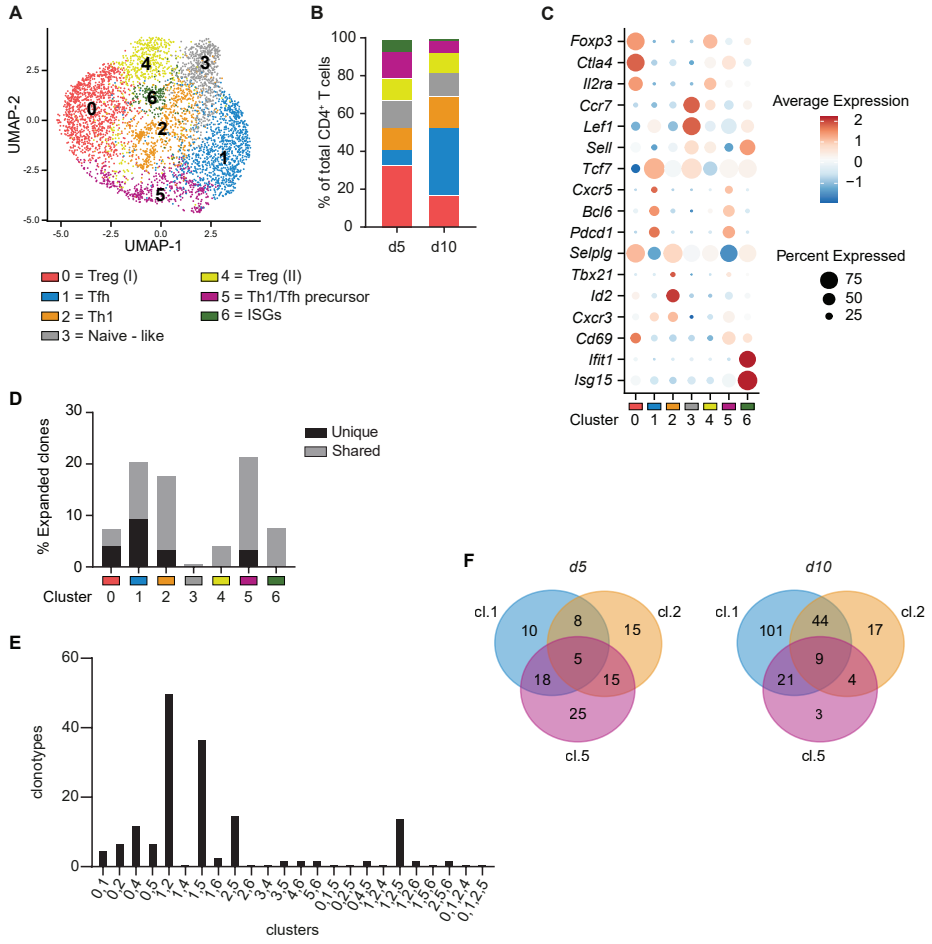

Figure 3. Identification of a common precursor for Th1 and Tfh cells in vaccinated mice. (A) UMAP projection of CD4^{+} T-cell clusters identified by scRNAseq of CD3^{+} CD44^{hi} CD62L^{low} T cells isolated from the dLN of mice at days 5 and 10 after vaccination with the MHC-II plasmid. (B) Bar plot depicting cluster distribution per time point. (C) Average mRNA expression level of indicated differentiation-associated genes and percentage of positive cells per cluster. (D) Frequency of expanded TCR clones (>1 cell per clone) per cluster. Black: TCR clones unique to one cluster; grey: TCR clones shared between two or more clusters. (E) Quantification of clonotypes shared between two or more indicated clusters. (F) Venn diagram depicting TCR sharing between Tfh cells from cluster (cl.) 1, Th1 cells from cl. 2 and Th1/Tfh precursor cells from cl. 5 derived at day 5 (left) or day 10 (right) after vaccination.

To determine whether Th1/Tfh precursor cells arise not only after vaccination, but also during infection, we analyzed previously published scRNAseq data from polyclonal GP66-tetramer$^+$ CD4$^+$ T cells isolated from spleens of mice infected with either acute LCMV-Armstrong or chronic LCMV-clone 13[54] (Figure 4A, Table S2). To identify corresponding cell states across datasets, we aligned the transcriptional profile of Tfh (cluster 1), Th1 (cluster 2) and Th1/Tfh precursor cells (cluster 5) defined in our vaccination model with the LCMV dataset using module scoring. Following LCMV infection, we detected Tfh cells and two Th1 clusters (Figure S4A-C). Th1 cells were prominent on day 8, whereas Tfh cells were more abundant on day 21 (Figure 4A). Both Th1 clusters expressed classical Th1-associated genes including *Cxcr6, Tbx21, Id2,* and *Prf1,* but were distinguished by differential expression of either *Gzma* and *Gzmb* (Th1 Gzmb$^+$ cluster) or *Prdm1, Eomes*, and *Gzmk* (Th1 Prdm1$^+$ cluster) (Figure S4A). The Tfh cluster expressed characteristic genes including *Cxcr5, Pdcd1, Il21 and Bcl6* (Figure S4A). Importantly, following both acute and chronic LCMV infection, we identified a population enriched for the transcriptional signature of the Th1/Tfh precursor cluster defined in our vaccination setting (Figure 4A, Figure S4D). This population was present under both infection conditions, but was more abundant at day 8 after acute infection (Figure 4A). Examination of the transcriptional profile revealed that approximately two-thirds of the genes differentially expressed in our vaccine-induced Th1/Tfh precursors (1,074 out of 1,576 genes) were also significantly enriched in the LCMV-induced Th1/Tfh precursor population (Figure 4B). To quantitatively assess transcriptional similarity between these two populations, we correlated average gene-expression values of their unified gene signature (Table S3) and observed a remarkably strong correlation (r = 0.94; Figure 4C). This concordance was particularly evident for transcripts that define this precursor state, including *Tcf7, Slamf6*, *Pdcd1*, *Cxcr3*, *Cxcr5*, *Tbx21* and *Bcl6*, as well as *Ldha* and *Gpr183*, which have been linked to the acquisition of stem-like properties in CD4$^+$ T cells[45].

In addition to this early Th1/Tfh precursor population, we also found the previously described *Slamf6*$^+$ *Tcf7*$^+$ *Bcl6*^{low} memory-precursor cluster[49,54] to be specifically enriched at day 21 post-chronic LCMV infection (Figure 4A, Figure S4A). A clonal relationship between this population and Th1 and Tfh cells has been documented[54]. Comparison of its gene signature (Table S3) with that of our vaccine-induced Th1/Tfh precursor revealed a more limited overlap (280 shared genes with FDR < 0.05; Figure 4D), likely reflecting differences in inflammatory context (acute vaccination versus chronic infection) and sampling time points. Nevertheless, the overall transcriptional correlation between the two populations was high (r = 0.84), particularly with respect to transcripts defining the Th1/Tfh precursor phenotype (Figure 4E). This chronic LCMV-induced memory-precursor population also shares a core gene signature with stem-like CD4$^+$ T cells in cancer that retain Th1 and Tfh differentiation potential[49]. Consistent with this relationship, the signature of stem-like CD4$^+$ T cells in cancer[49] was significantly enriched in our vaccine-induced Th1/Tfh precursor cells (Figure 4F), indicating that these cells adopt a stem-like transcriptional program.

To determine whether the Th1/Tfh precursor state was conserved across different infectious contexts, we next analyzed previously published data from *Plasmodium*-specific TCR transgenic CD4$^+$ T cells responding to malaria infection, a model in which a common activated precursor state preceding Th1 or Tfh differentiation has also been described[4]. We extracted the gene signature of malaria-induced Th1/Tfh precursors (1,626 dynamic genes; D statistic >50; Table S4) and found significant enrichment of this signature in our vaccine-induced Th1/Tfh precursor population (Figure 4G), with 1,515 of the 1,625 genes showing significantly enrichment in both datasets (FDR < 0.05). Altogether, these findings demonstrate that antigen-specific CD4$^+$ T cells transit through a conserved, uncommitted Th1/Tfh precursor state prior to differentiation into Th1 or Tfh effector lineages after vaccination or infection with acute and chronic LCMV or malaria. This precursor population further shares a core stem-like transcriptional signature with memory precursors arising specifically during chronic LCMV infection and with stem-like CD4$^+$ T cells in tumors, consistent with a shared capacity to sustain differentiation toward both Th1 and Tfh lineages across diverse immune response settings.

Th1/Tfh precursors are proliferative and co-express Th1- and Tfh-related transcription factors and chemokine receptors

To gain deeper insights into the transcriptional programs underlying Th1 and Tfh cell differentiation, we performed differential gene expression analysis between Tfh (cl.1) and Th1 (cl.2) cells generated after vaccination. Gene signatures of the two T-helper subsets were characterized by lineage-defining transcription factors, including *Tbx21*, *Id2*, *Bhlhe40* and *Prdm1* for Th1 cells, and *Bcl6*, *Tox* and *Tox2* for Tfh cells, which validated the robustness of our dataset (Figure 5A; Tables S5 and S6)[24,44,55,56]. Comparison of the transcriptional profile of the common Th1/Tfh precursor cells (cl. 5) to that of naive-like cells (cl. 3) revealed the characteristics of this population (Figure 5B). Cluster 5 cells expressed many genes associated with either Th1 or Tfh fate, including transcription factors *Tbx21*, *Bhlhe40*, *Prdm1* and *Bcl6*, as well as chemokine receptors *Cxcr3* and *Cxcr5*. These transcripts were co-expressed within the same cells and enriched in cluster 5, as shown by the positive correlation in expression of e.g. *Tbx21* and *Cxcr5*, or *Tbx21* and *Bcl6* (Figure S5A, B). In addition, cells of cluster 5 displayed upregulation of *Mki67*, indicating active cell division, and multiple costimulatory receptors including *Icos*, *Tnfrsf8* (encoding CD30), *Tnfrsf9* (encoding CD137, alias 4-1BB), *Tnfrsf18* (encoding CD357, alias GITR), and *Tnfrsf1b* (encoding CD120b, alias TNFR2) (Figure 5B).

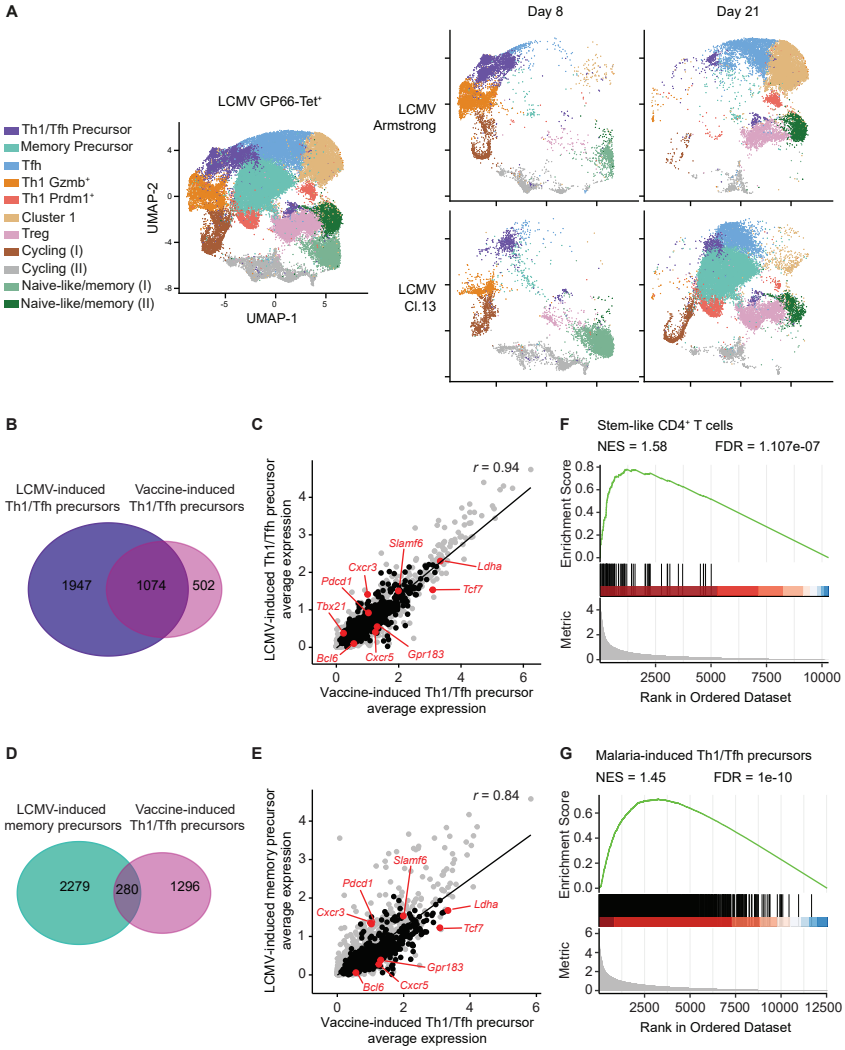

Figure 4. The Th1/Tfh precursor population is conserved across different infection models. (A) Left: UMAP projection of splenic GP-66 Tet+ CD4+ T cells derived from mice infected with LCMV-Armstrong or LCMV-clone 13 at day 8 and day 21 post-infection. Data were re-analyzed from Xia et al.[54]. Right: Deconvolution of UMAPs per infection model and time point. (B, D) Venn diagrams showing the overlap between genes significantly enriched (FDR < 0.05) in vaccine-induced Th1/Tfh precursors and either LCMV-induced Th1/Tfh precursors (B) or LCMV-induced memory precursors (D). (C, E) Scatter plots comparing the average expression of genes significantly enriched (FDR < 0.05) in vaccine-induced Th1/Tfh precursors with their expression in LCMV-induced Th1/Tfh precursors (C) or LCMV-induced memory precursors (E). Spearman's correlation coefficient (r) was calculated to quantify transcriptional similarity. Grey dots represent all genes significantly enriched (FDR < 0.05) in either population (union of enriched genes); black dots indicate genes significantly enriched in both populations (shared enriched genes); red dots highlight selected genes of interest. (F, G) Gene set enrichment analysis of gene signatures of stem-like CD4+ T cells (from Cardenas et al.[49]) (F) and malaria-induced Th1/Tfh precursor cells (from Lönnberg et al.[4]) (G) in vaccine-induced Th1/Tfh precursor cells. A total of 59/62 and 1,515/1,625 genes, respectively, overlapped with the ranked gene list.

To map the formation of common Th1/Tfh precursor cells by flow cytometry, we followed the response of TCR transgenic OTII cells that recognize $OVA_{323-339}$ peptide in the context of MHC-II. $CD45.1^+$ OTII cells were labeled with carboxyfluorescein succinimidyl ester (CFSE) to track proliferation and adoptively transferred into $CD45.2^+$ recipient mice. One day later, recipient mice received one dose of a modified MHC-II DNA vaccine encoding both PADRE and $OVA_{323-339}$ epitopes (MHC-II:OVA; Figure S5C). This vaccine simultaneously induced a transgenic OTII $CD4^+$ T-cell response to the OVA epitope and an endogenous $CD4^+$ T-cell response to the PADRE epitope (Figure S5D, E), enabling us to compare the differentiation trajectories of these two responder cell populations. Because transferred naive OTII cells are present at relatively high frequency, this system allowed us to analyze their early activation state, whereas endogenous PADRE tet^+ $CD4^+$ T cells became detectable by tetramer staining only at day 4 post-vaccination (Figure S5F, G). We therefore monitored the $CD4^+$ T-cell response in the dLNs from day 1 to 5 post-vaccination. Proliferation of OTII cells was initiated by day 3, and by day 4 the majority of OTII cells were actively dividing, with fraction having already undergone at least seven divisions (Figure 5C, Figure S5H). Accordingly, the frequencies of both OTII cells and PADRE tet^+ $CD4^+$ T cells were significantly increased by day 4 post-vaccination (Figure S5F, G). At day 3, concurrent with the start of cell division, OTII cells upregulated the activation marker CD44, as well as the chemokine receptor CXCR5 (Figure 5D, Figure S5I) that is commonly used as a marker of Tfh precursors[57-59]. Interestingly, $CD44^{hi}$ $CXCR5^+$ OTII cells also expressed high levels of CXCR3 (Figure 5E, F), a chemokine receptor that among $CD4^+$ T cells is thought to be specifically upregulated on Th1 precursors[60]. Consistent with our scRNAseq data, $CD44^{hi}$ $CXCR5^+$ $CXCR3^+$ OTII cells co-expressed T-bet and BCL6 proteins (Figure 5G, H). Within the endogenous $CD4^+$ T-cell pool, PADRE tet^+ $CD44^{hi}$ CD4 T cells also co-expressed CXCR5, CXCR3, T-bet and BCL6 at day 4 post-vaccination (Figure 5E, G; Figure S5J-L). In addition, $CD44^{hi}$ OTII cells expressed higher levels of PD-1 compared to $CD44^{low}$ cells (Figure S5M), consistent with our results for endogenous cells (Figure 2E).

TCR transgenic T cells all have the same affinity and may therefore have an intrinsic predisposition to a specific differentiation trajectory[7]. Next to low affinity OTII cells, we also used SMARTA $CD4^+$ T cells that have a transgenic, high affinity TCR recognizing the GP_{61-80} epitope of LCMV in the context of MHC-II[60], in conjunction with a modified MHC-II vaccine that encodes both the PADRE and GP_{61-80} epitopes (Figure S5N, O). SMARTA $CD4^+$ T cells also differentiated into $CD44^{hi}$ precursor cells co-expressing CXCR3, CXCR5, T-bet and BCL6, as observed at day 4 post-vaccination (Figure S5O). Obtaining the same results with low and high affinity TCR transgenic $CD4^+$ T cells, as well as PADRE-specific endogenous, polyclonal $CD4^+$ T cells indicates that the formation of the Th1/Tfh precursor cell pool is independent of TCR affinity. The collective data thus establish that activated $CD4^+$ T cells initially form a proliferative pool of common Th1/Tfh precursors with a distinct marker profile that can differentiate into either Th1 or Tfh cells, independent of TCR affinity.

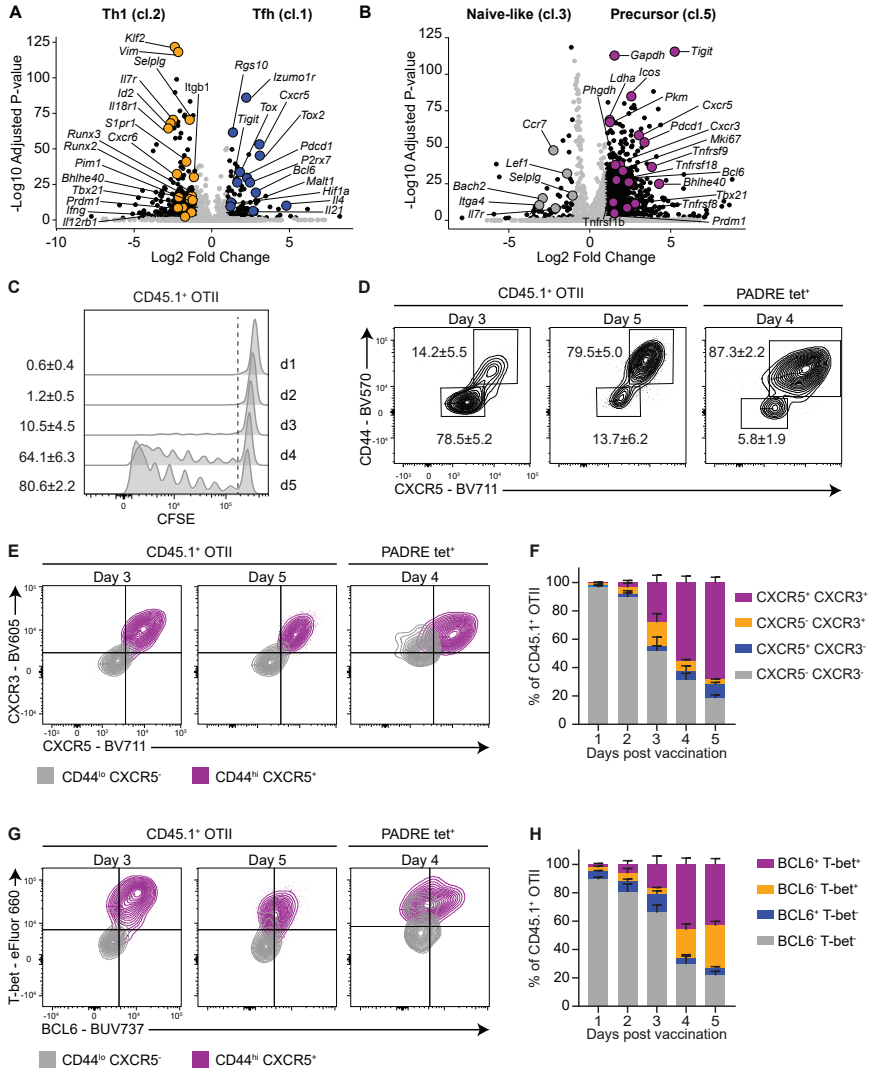

Figure 5. Common Th1/Tfh precursors co-express Th1- and Tfh markers at protein level. (A, B) Volcano plots depicting differential gene expression derived from scRNAseq data of vaccinated mice, comparing Tfh cells (cl. 1) versus Th1 cells (cl. 2) (A), or naive-like CD4$^+$ T cells (cl. 3) versus Th1/Tfh precursor cells (cl. 5) (B). Black dots depict genes with fold change < -1 or > 1 and adjusted P<0.05. (C) Mice received OTII cells, were vaccinated once with MHC-II:OVA vaccine, dLNs were harvested and cells analyzed by flow cytometry. Histograms depicting divisions of vaccine-activated, adoptively transferred OTII cells, as measured by CFSE dilution. Numbers indicate frequency of divided OTII cells (mean ± SD). (D) Representative CD44 and CXCR5 protein expression on CD45.1$^+$ OTII or PADRE tet$^+$ CD4$^+$ T cells, measured in dLNs at indicated days post-vaccination. (E, G) Representative overlays of CXCR5 and CXCR3 (E) or T-bet and BCL6 (G) protein expression in CD44^{lo} CXCR5$^-$ (gray) and CD44$^+$ CXCR5$^+$ (purple) CD45.1$^+$ OTII or PADRE tet$^+$ CD4$^+$ T cells. (F, H) Proportion of CD45.1$^+$ OTII responder cells expressing CXCR5 and CXCR3 (F) or T-bet and BCL6 (H) in the dLNs at the indicated days post-vaccination (N=3-5 per time point; representative of 3 independent experiments). Graphs depict mean ± SD.

Specific costimulatory signals drive formation of the common Th1/Tfh precursor pool and subsequent Th1 or Tfh differentiation

Having identified the common Th1/Tfh precursor, we were interested in the costimulatory signals that drive its formation and further differentiation. It is known that Th1 and Tfh differentiation rely on specific costimulatory molecules[61], but how and when these signals operate during the step-wise differentiation trajectories from the naive T cell, via the common Th1/Tfh precursor into the Th1 and Tfh lineages has not been established yet. We first examined the impact of costimulatory receptor CD28 that synergizes with the TCR/CD3 complex in initiating T-cell activation, but is also required to maintain both Th1 and Tfh cells[62]. To this end, CD28 costimulation was inhibited by infusion of blocking monoclonal antibodies (mAbs) against both CD80 and CD86 in mice that received OTII cells and MHC-II:OVA vaccination once. This intervention did not significantly affect the overall frequency of OTII cells in dLN at day 5 after vaccination (Figure S6A), but did reduce the frequency of CD44$^+$ CXCR3$^+$ CXCR5$^+$ OTII Th1/Tfh precursor cells (Figure 6A). CD80 and CD86 blockade also reduced the frequency of total PADRE tet$^+$ CD4$^+$ T cells (Figure 6B), suggesting that CD28 costimulation promotes formation of the Th1/Tfh precursor pool by supporting clonal expansion of recently activated CD4$^+$ T cells, in line with its role during initial T-cell priming[63]. Because CD80 and CD86 have different affinities for CD28[64] and distinct roles in the maturation of Tfh cells in germinal centers[65], we also investigated whether they had independent impact on the CD4$^+$ T-cell differentiation trajectory. Single blockade of either CD80 or CD86 did not affect the generation of CXCR3$^+$ CXCR5$^+$ OTII Th1/Tfh precursor cells (Figure 6C), nor the expansion and initial Th1 or Tfh bifurcation of PADRE$^+$ CD4$^+$ T cells (Figure 6D; Figure S6B-D), indicating that CD80 and CD86 are redundant in promoting formation of the Th1/Tfh precursor pool.

We next evaluated the impact of CD40 and ICOS costimulation on the CD4$^+$ T-cell differentiation trajectory towards and from the Th1/Tfh precursor state. CD40:CD40L interaction has been reported to promote both Th1 and Tfh function[66-68] and ICOS:ICOSL interaction is important for Tfh differentiation[58,66,68-70]. Blockade of CD40L or ICOSL did not affect the frequency of CD44$^+$ CXCR5$^+$ CXCR3$^+$ OTII precursor cells, total PADRE tet$^+$ CD4$^+$ T cells, or total OTII cells (Figure 6E; Figure S6E, F), indicating that CD40 and ICOS costimulation were not required for formation of the Th1/Tfh precursor pool. However, among PADRE tet$^+$ cells, CD40L blockade significantly reduced the frequency of Th1 cells, while not affecting the frequency of Tfh cells (Figure 6F, G). Conversely, blockade of ICOSL lowered the frequency of Tfh cells, while not affecting the frequency of Th1 cells (Figure 6F, G). Because early CXCR5 and BCL6 expression has been reported to depend on ICOS costimulation[57,58,71], we further validated our results for ICOS blockade using CRISPR/Cas9-mediated knockout of ICOS in OTII T cells. Mice received naive OTII cells expressing either a control gRNA (Ctrl) or a pool of three gRNAs against ICOS (ICOS^{ko}), and were subsequently vaccinated with MHCII:OVA. Whereas all activated CD44^{hi} Ctrl OTII cells upregulated ICOS, ICOS expression was abrogated in 75% of ICOS^{ko} OTII cells, confirming effective genetic disruption (Figure S6G). We restricted our analysis to bona fide

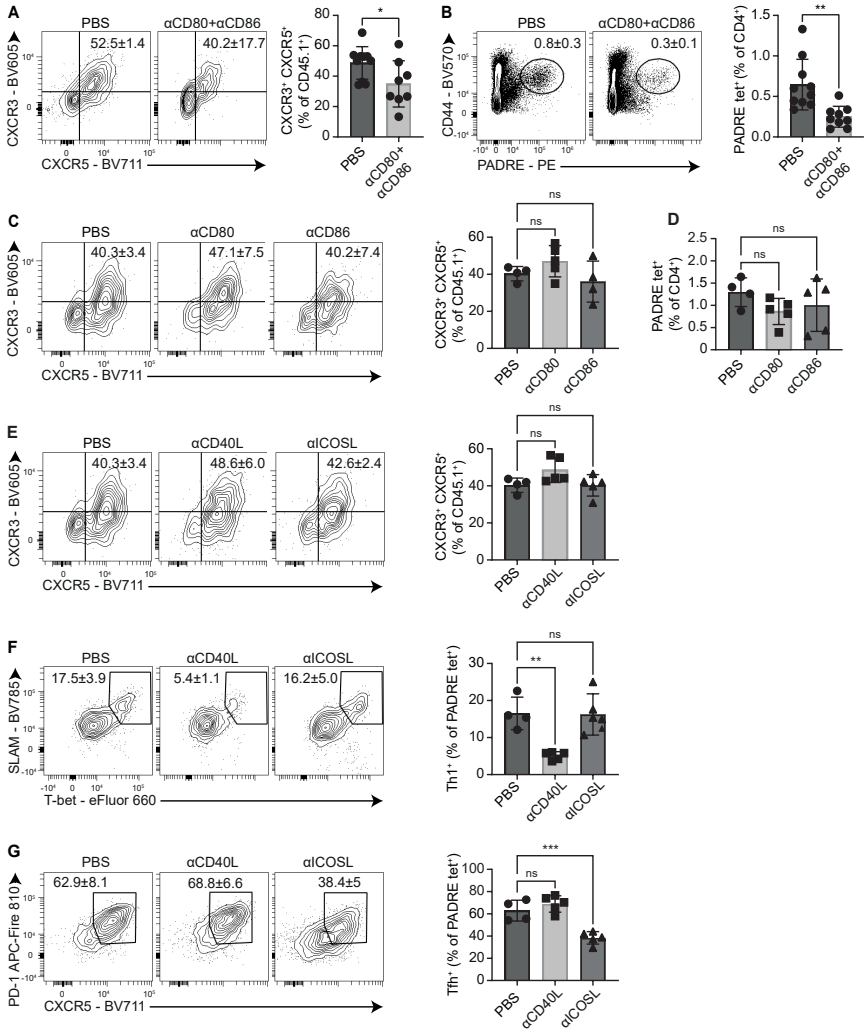

Figure 6. CD28 costimulation promotes formation of the Th1/Tfh precursor pool, from which CD40 or ICOS drive Th1 or Tfh differentiation, respectively. OTII cells were adoptively transferred in recipient mice, which were vaccinated one day later with a single dose of MHC-II:OVA vaccine and treated with blocking monoclonal antibodies (mAbs) against the indicated costimulatory ligands or PBS (control). dLNs were harvested at day 5 after vaccination and analyzed by flow cytometry. Representative plots and quantification of frequencies of cells expressing indicated markers are shown. (A, B) Frequencies of CXCR3$^+$ CXCR5$^+$ CD45.1$^+$ OTII cells (A) and CD45.2$^+$ PADRE tet$^+$ CD4$^+$ T cells in mice treated with a combination of blocking mAbs to CD80 and CD86 (B) (N=9-10 per group; data pooled from 2 independent experiments). Unpaired Student's t-test. (C, D) Frequencies of CXCR3$^+$ CXCR5$^+$ CD45.1$^+$ OTII cells (C) and CD45.2$^+$ PADRE tet$^+$ CD4$^+$ T cells (D) in mice treated with blocking mAbs to either CD80 or CD86. (E, F, G) Frequencies of CXCR3$^+$ CXCR5$^+$ precursor CD45.1$^+$ OTII T cells (E), CD45.2$^+$ PADRE$^+$ SLAM$^+$ T-bet$^+$ Th1 (F) and CD45.2$^+$ PADRE$^+$ CXCR5$^+$ PD-1$^+$ Tfh (G) cells in mice treated with blocking mAb to either CD40L or ICOSL. (C-G) N=4-5 per group; data are representative of at least two independent experiments. One-Way ANOVA with Dunnett's post hoc test was used to correct for multiple testing when comparing inhibitory conditions to control. All graphs show mean ± SD.

ICOS-deficient cells within the ICOS^{ko} OTII population and found that activated CD44^{hi} ICOS-deleted OTII cells effectively upregulated CXCR5 and BCL6 expression compared to their naive CD44^{low} counterpart, although their expression levels were slightly lower than in CD44^{hi} Ctrl OTII cells (Figure S6H, I). Consistent with this, the frequency of CXCR3^{+} CXCR5^{+} cells was comparable between ICOS-deleted and Ctrl OTII cells (Figure S6J), confirming that early CXCR5 and BCL6 upregulation, and the resulting formation of the Th1/Tfh precursor pool, occur independently of ICOS signaling. In line with our results using ICOSL antibody blockade, CRISPR/Cas9-mediated deletion of ICOS in OTII cells impaired Tfh differentiation (Figure S6K), without affecting Th1 cells (Figure S6L). Altogether, these data provide a scenario wherein CD28 costimulation driven by either CD80 or CD86 promotes formation of the Th1/Tfh precursor cell pool, whereafter the precursors are driven into Th1 cells with the aid of CD40-CD40L interactions and into Tfh cells with the aid of ICOS-ICOSL interactions.

Th1/Tfh precursors differentiate into either Th1 or Tfh cells in a second priming step on cDC1s or B cells, respectively

We next examined the role of cDC1s and B cells in guiding the differentiation of Th1 and Tfh cells from the Th1/Tfh precursor. The role of cDC1s was determined by using *Batf3*$^{-/-}$ mice on a C57BL6/J background[13,72], which display complete loss of migratory cDC1s (MHCII^{hi} CD11c^{int} CD103^{+} XCR1^{+}) and partial loss of resident cDC1s (MHCII^{int} CD11c^{hi} XCR1^{+}) (Figure S7A-F). The role of B cells was determined by effective B-cell depletion using a mAb to CD20 prior to vaccination (Figure S7G). In both experimental set-ups, OTII cells were adoptively transferred, the MHC-II:OVA vaccine was administered once, and responses were read out in the dLNs by flow cytometry at day 5 after vaccination. Neither *Batf3*-deficiency (Figure S7H, I), nor B cell depletion (Figure S7L, M) affected the clonal expansion of endogenous PADRE tet^{+} CD4^{+} T cells or OTII cells. Formation of CD44^{+} CXCR3^{+} CXCR5^{+} Th1/Tfh precursor cells was also unaffected in mice lacking these APCs (Figure 7A, B). However, *Batf3*$^{-/-}$ mice showed a decrease in the generation of Th1, but not Tfh cells, while B-cell depleted mice showed a decrease in the generation of Tfh, but not Th1 cells. This was the case for both endogenous PADRE tet^{+} CD4^{+} T cells (Figure 7C-F) and for exogenous OTII cells (Figure S7J-K, N-O). Altogether, these data indicate that CD28-dependent formation of the Th1/Tfh precursor pool is instructed by APCs other than cDC1s and B cells, most likely cDC2s. Thereafter, in a second step of priming, the precursor cells are instructed for Th1 differentiation on cDC1, as driven by CD40 costimulation, or for Tfh differentiation on B cells, as driven by ICOS costimulation.

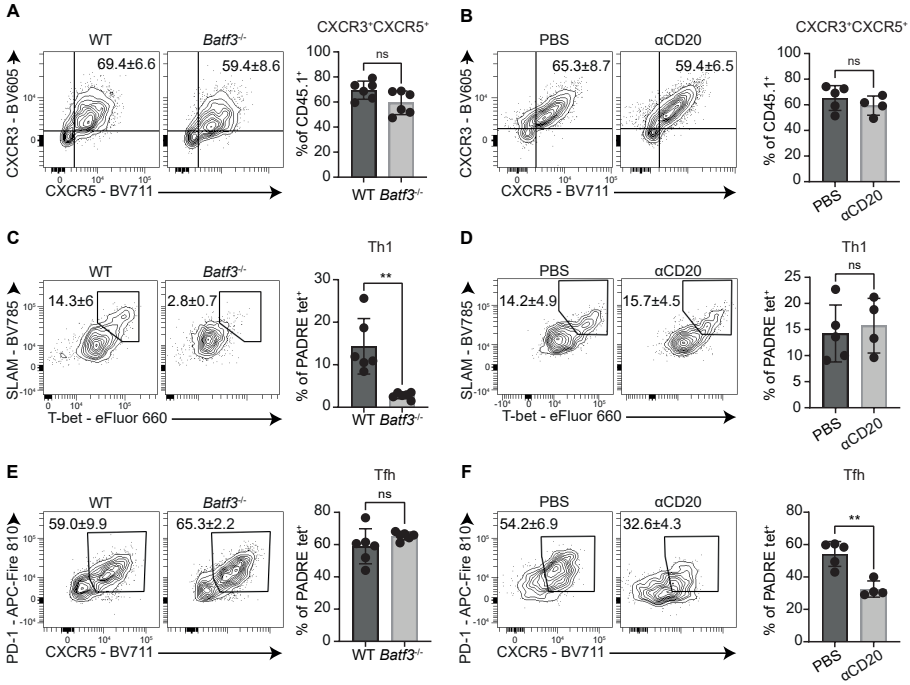

Figure 7. Th1 or Tfh differentiation from the common Th1/Tfh precursor is driven by interactions with cDC1s or B cells, respectively. Wild-type (WT) or Batf3$^{-/-}$ mice received OTII cells, were vaccinated once with MHC-II:OVA vaccine and were treated with depleting mAb to CD20 or PBS (control) as indicated. At day 5 after vaccination, cells from dLN were analyzed by flow cytometry. Representative plots and quantification of frequencies of cells with indicated markers are shown. (A, B) Flow cytometry plots and quantification of CXCR3^{+} CXCR5^{+} CD45.1^{+} OTII cells in the dLN of WT versus Batf3$^{-/-}$ mice (A), or WT mice that were treated with B-cell depleting anti-CD20 mAb or PBS (control), two days before vaccination (B). (C-F) Flow cytometry plots and quantification of SLAM^{+} T-bet^{+} Th1 (C, D) or CXCR5^{+} PD-1^{+} Tfh (E, F) PADRE tet^{+} CD4^{+} T cells in WT versus Batf3$^{-/-}$ mice (C, E), or WT mice treated with anti-CD20 mAb or PBS (D, F). All graphs depict mean ± SD (N=6 per group in A, C, E; N=4-5 per group in B, D, F). A-F, Unpaired Student's t-test.

Discussion

In this study, we characterize a mouse vaccination model that enables longitudinal tracing of Th1 and Tfh differentiation from endogenous, polyclonal CD4$^+$ T cells. By integrating single-cell transcriptomics, TCR sequencing, and high-dimensional flow cytometry, we demonstrate that individual antigen-specific CD4$^+$ T cell clones transiently pass through a common, highly proliferative Th1/Tfh precursor state before committing to either Th1 or Tfh effector phenotypes. This precursor population exhibits features of recent activation and stem-like potential, marked by expression of CD69, PD-1, TCF1 and SLAMF6, while simultaneously co-expressing key Th1- and Tfh-associated molecules at both the mRNA and protein levels, including CXCR3, T-bet, CXCR5, and BCL6. The vaccine-induced Th1/Tfh precursor state aligns transcriptionally with analogous populations identified during malaria[4] and both acute and chronic LCMV infection[55]. In addition, it shares a core gene signature with memory precursors and stem-like CD4$^+$ T cells described in chronic LCMV infection and tumors, respectively[49,54]. Interestingly, its transcriptional program also resembles that of stem-like LCMV-specific CD8$^+$ T cells[73-75], suggesting that CD4$^+$ and CD8$^+$ T cell lineages can transiently form similar intermediate states during immune responses.

During priming in secondary lymphoid organs, CD4$^+$ T cells have multiple contacts with different APCs. This is most explicit for Tfh formation in which both cDCs and B cells play a role. Initial priming typically occurs in the T-cell zone by cDC2s[76-78], giving rise to activated CD4$^+$ T cells that upregulate CXCR5 and are commonly referred to as pre-Tfh cells. These cells migrate along a CXCL13 gradient towards the border between the T- and B-cell zone or the interfollicular region (IFR)[19,79], where they receive additional stimulation that promote entry into the B-cell follicle and completion of Tfh differentiation[79-81]. Although early expression of CXCR5 and PD-1 on activated CD4$^+$ T cells is often considered indicative of Tfh commitment, not all CXCR5$^+$ PD-1$^+$ CD4$^+$ T cells ultimately become Tfh cells[79,81]. In contrast to CXCR5, CXCR3, a chemokine receptor responsive to IFN-induced CXCL9 and CXCL10, has classically been associated with Th1 differentiation[82]. This chemokine receptor also guides activated CD4$^+$ T cells towards the IFR[82]. At this site, CD4$^+$ T cells can provide help to CD8$^+$ T cells through cognate interactions with the same cDC1[5,83,84], but they can also interact with B cells[79]. Consistent with co-expression of CXCR3 and CXCR5 on the common Th1/Tfh precursor as documented here, CXCR3 expression has previously been detected on cells with a Tfh-like phenotype[7,26]. CXCR3$^+$ CXCR5$^+$ PD-1^{low} cells, as well as Tfh-like cells that share chemokine receptor and transcription factor expression with Th2 or Th17 cells, have also been detected in human peripheral blood[85]. CXCR3$^+$ Tfh-like cells have been associated with improved responses to influenza vaccination and correlate with neutralizing antibodies in HIV controllers[86-88]. These circulating Tfh-like cells express CD62L and CCR7, suggesting that they are in a less differentiated or memory-like state[85] and remain responsive to antigenic stimulation. Our definition of a CXCR3$^+$ CXCR5$^+$ Th1/Tfh precursor state thus provides a mechanistic explanation for these dual phenotypes, revealing a flexible intermediate state

that can give rise to both Th1 and Tfh lineages and likely corresponds to previously described pre-Tfh cells. We postulate that the differentiation fate of these Th1/Tfh precursors is guided by the relative dominance of chemokine cues, with CXCR5 directing cells toward B cells for Tfh differentiation and CXCR3 guiding them to cDC1s for Th1 differentiation.

Our data also clarify the step-wise differentiation process in which responder CD4$^+$ T cells rely on interactions with different antigen presenting cells and the costimulatory signals they provide. Formation of Th1/Tfh precursors depends on CD28-signalling via either CD80 or CD86, likely reflecting the essential role of CD28 in driving clonal expansion of responder T cells[63]. Consistent with a chemokine- and costimulation-guided model, we found that cDC1 and CD40:CD40L interaction are required for Th1 differentiation from the common precursor, whereas B cells and ICOS costimulation are required for Tfh differentiation. CD40 signaling in cDC1 is associated with upregulation of costimulatory molecules such as CD70, expression of IL-12 and apoptosis resistance[18,89,90]. CD40 is also critical in the maintenance of Tfh and GC responses[66], and it was somewhat surprising that blockade did not affect Tfh cell differentiation in our model. Similarly, CD86 is known to promote Tfh differentiation[65], but we did not find any effects of single CD86 blockade. This may be explained by the fact that we focused on early differentiation stages, prior to the establishment of germinal centers, when CD40 and CD86 signals may be trivial or compensated for. In addition to cDC1, CD40 signals and CXCR3-attracting chemokines can also be delivered by monocyte-derived (Mo)DCs present within the IFR[91]. This aligns with our recent data showing that CD4$^+$ T cells and MoDCs communicate in a CD40-dependent feed-forward loop to enforce Th1 effector differentiation[40], which can be mediated by IL-12[92,93].

The formation of a Th1/Tfh precursor thus allows immune system flexibility in tailoring host protection to ongoing infections. Different viral infections can result in different Th1/Tfh ratios, which are reinforced through regulatory feedback loops that modulate the expression of T-bet or BCL6[5,10,21,94]. For example, acute LCMV and influenza infections differentially depend on T-bet expression[95], whereas vesicular stomatitis virus (VSV) induces a higher Tfh/Th1 ratio than LCMV[10]. Given that Th1/Tfh precursors arise across diverse infection models, their subsequent differentiation is likely context-dependent, with the relative balance of T-bet and BCL6 expression determining commitment to either the Th1 or Tfh lineage[24].

Our data further demonstrate that Th1/Tfh precursors are not restricted to vaccination or acute infection, but share a core gene signature with stem-like CD4$^+$ T cells, including *Tcf7*, *Pdcd1*, *Slamf6*, *Ldha*, and *Gpr183*, underscoring their conserved and flexible nature. Stem-like CD4$^+$ T cells, previously identified in transplantation rejection and cancer, have been shown to act as key intermediates that can re-establish Th1 effector differentiation[45,49]. Interestingly, a pan-cancer analysis across 21 tumor types identifies a tumor-enriched CD4$^+$ T-cell population predicted to be tumor-specific and characterized by both Th1- and Tfh-associated gene expression[96], which

qualifies as Th1/Tfh precursor cells. Together, these findings underscore the need to generally acknowledge the Th1/Tfh precursor cell state and to fully define the developmental cues for either Th1 or Tfh differentiation from this state.

Limitations of the study

A limitation of our study is that we did not directly test whether individual precursors are truly bipotent, which would require tracking of single $CXCR3^{+}CXCR5^{+}$ Th1/Tfh cells after adoptive transfer into recipient mice. In addition, given the transcriptional similarity between the Th1/Tfh precursor population, stem-like $CD4^{+}$ T cells, and memory-precursors arising during chronic LCMV-infection, future studies should determine whether Th1/Tfh precursor cells possess self-renewal and memory potential, and can therefore be functionally classified as stem-like.

Methods

Animal models

Mice were housed in individually ventilated cages (IVC) under specific pathogen free (SPF) conditions in groups of 2-4 mice per cage for males or 2-5 mice per cage for females. Mice received *ad libitum* access to water and standard laboratory chow diet. Ambient temperature was ~19-21°C and humidity 30-70%. Lighting was provided on a 12 h light/dark cycle. Eight-week-old male and female C57BL/6JRj mice were purchased from Janvier laboratories (Le Genest Saint Isle, France). OTII*CD45.1 (B6.SJL-PtprcaPepcbTg(TcraTcrb)425Cbn/CrlLumc) on a C57BL/6JRj background were bred in-house, and genotype was verified by flow cytometry. $Batf3^{-/-}$ (B6.129S(C)-Batf3tm1Kmm/J) on a C57BL/6J background and wild-type C57BL/6J control mice were obtained from The Jackson Laboratory. Mice were habituated for 1 week prior to the start of an experiment and only one sex was used per experiment. All mouse experiments were performed in accordance with institutional and national guidelines under license number AVD16497, and were approved by the Animal Welfare Body at Leiden University Medical Center.

DNA tattoo vaccination

The cDNAs encoding the MHC-II, MHC-II:OVA, MHC-IIGP(61-80) and control sequences used for DNA vaccination were expressed in a pVAX1 plasmid vector. MHC-II and control vaccines have previously been described[34,37]. MHC-II:OVA and MHC-II-GP(61-80) vaccines were generated by excising the cassette encoding the MHC-II epitopes (p30, PADRE, HIV $Nef_{56\text{-}68}$) from the MHC-II vaccine cDNA with HindIII and XhoI restriction enzymes, and replacing it with a gBlock containing the MHC-II cassette linked to nucleotide sequences encoding $OVA_{323\text{-}339}$ (ISQAVHAAHAEINEAGR) or LCMV-Armstrong derived $GP_{61\text{-}80}$ (GLKGPDIYKGVYQFKSVEFD) and a GPGPGPG linker on both ends as for the original MHC-II vaccine.

For intraepidermal DNA tattoo vaccination[34,41], mice were anesthetized using isoflurane (Alvira Isoflutek 1000mg/g, induction phase: 4% isoflurane, airflow 0.8 l/min; maintenance phase: 2% isoflurane, airflow 0.4 l/min) and the right hind leg of mice was depilated using Veet containing limonene (Reckitt Benckiser). Subsequently, 15 µl of a 2 mg/ml plasmid DNA in H_2O was tattooed into the skin with a Permanent Make Up tattoo machine (Cheyenne, MT Derm GmbH) using a sterile disposable needle with a needle depth of 1 mm. Tattooing was performed for 45 sec, oscillating at a frequency of 100 Hertz. Mice were vaccinated on day 0, 3, and 6 unless otherwise indicated in the relevant figure legend or Results section, and alternating between the internal or external upper part of the right hind leg.

Adoptive T-cell transfer

For adoptive transfer, spleens were isolated from 8- to 12-week-old, sex matched OTII*CD45.1 mice after euthanasia. Spleens were mechanically disrupted and passed through a 70 µM Falcon strainer (Corning). Subsequently, single cell suspensions were incubated in red blood cell (RBC) lysis buffer (Santa Cruz) for 5 min at room temperature. $CD4^+$ T cells were isolated by negative selection using a $CD4^+$ T-cell isolation kit (Miltenyi) according to the manufacturer's protocol. If indicated, purified OTII*CD45.1 $CD4^+$ T cells were labelled with 2.5 µM CFSE (Invitrogen) for 10 min at 37°C. Free CFSE was then quenched by adding at least five times excess of Iscove's modified Dulbecco's medium (IMDM) with L-glutamine (Capricorn) and 10% fetal bovine serum (FBS), 100 units/ml penicillin and 100 mg/ml streptomycin (Gibco), and resting cells for 5 min at room temperature. Cell purity (>90%) and CFSE-labelling were checked for each experiment by flow cytometry using the following monoclonal antibodies (mAbs) against mouse molecules: 1:100 CD45.1 BUV395 (clone A20, BD Biosciences), 1:200 CD4 BUV805 (clone GK1.5, BD Biosciences), 1:200 TCRvα2 BV421 (clone B20.1),TCRvβ5.1/5.2 PE-Cy7 (clone MR9-4), 1:100 CD44 BV570 (clone IM7), and 1:100 CD62L PE-Fire 810 (clone W18021D; all BioLegend). C57BL/6JRj mice received 0.1 x 10^6 or 0.5 x 10^6 or 1 x 10^6 OTII*CD45.1 cells in 100 µl Hank's Balanced Salt Solution (HBSS) depending on the day of read out, or 5 x 10^5 purified SMARTA*GFP (B6.Cg-Ptprca Pepcb Tg(TcrLCMV)1Aox/PpmJx) cells in 100 µl HBSS, kindly provided by Dr. K. Jobin and Prof. W. Kastenmüller (University of Würzburg, Germany), by retro-orbital i.v. injection under isoflurane anesthesia.

When indicated, purified OTII*CD45.1 $CD4^+$ T cells were genetically modified using Cas9 RNPs (protocol adapted from refs.[97,98]). Briefly, purified cells were electroporated with complexes of *S. pyogenes* Cas9 nuclease V3 (Integrated DNA Technologies) and control or ICOS targeting gRNAs in P4 Primary Cell solution (Lonza) using a 4D Nucleofector X-16 Strip unit (Lonza) with DN100 settings. A combination of three guide sequences were used to target the genomic sequence of the *Icos* gene: #1 ACAATCGCATTTTTAACTGC; #2 TGGTCTTGGTGAGTTCGCAG; #3 GAGGTGGGTCAAAAATGGAC; whereas the following sequence was used as non-targeting control: GCACTACCAGAGCTAACTCA[97] (all from Integrated DNA Technologies). After electroporation cells were cultured for 24h in IMDM medium (Gibco) containing 10% FCS and

10 ng/mL recombinant IL-7 (Peprotech; 217-17), before transfer into recipient mice. Knockout efficiency was determined on day 5 or day 8 post-vaccination by flow cytometry. Only cells that lacked ICOS expression were analyzed for the $ICOS^{ko}$ group.

Antibody and reagent treatment of mice

All antibodies or reagents were injected intraperitoneally (i.p.). Mice received 250 µg depleting anti-CD20 mAb (MB20-11, BioXcell) at day -2. Mice with incomplete B-cell depletion were excluded from analysis. For blocking costimulatory ligands, mice received injections on days 0 and 3 post vaccination with 150 µg anti-CD40L mAb (MR-1, BioXcell), 200 µg anti-CD80 mAb (1G10, BioXcell), 200 µg anti-CD86 mAb (GL-1, BioXcell) or 200 µg anti-ICOSL mAb (HK5.3, BioXcell). FTY720 (Fingolimod, Cayman Chemicals) was dissolved in 96% ethanol at 20 mg/ml and prior to injection diluted in 0.9% NaCl. Mice received 25 µg FTY720 in 200 µl 0.9% NaCl at days 0, 3 and 6.

Cell isolation

On the day of readout, mice were euthanized and organs collected. Blood was collected by tail vein puncture or cardiac puncture. Erythrocytes were lysed by incubation in RBC lysis buffer (Santa Cruz) for 5 min at room temperature. Inguinal dLNs of the vaccination site were punched repeatedly with a 25G needle and incubated for 30 min at 37°C while shaking in 100 µg/ml Liberase TL (Roche) prepared in 500 ml DMEM. Enzymatic digestion was quenched by adding FBS-supplemented IMDM, and single cell suspensions prepared by mechanical disruption of dLNs through 70 µm Falcon strainers (Corning).

Flow cytometry

For cell surface staining, mAbs were diluted in FACS buffer (PBS + 2% FBS). Single cell suspensions were first incubated for 1 h at room temperature with 1:200 PE-conjugated PADRE tetramer (AKFVAAWTLKAA in I-A(b), NIH tetramer facility), and then for 30 min on ice with the following mAbs: 1:200 CD4 BUV805 (clone GK1.5), 1:200 PSGL1 BUV661 (clone 2PH1), 1:200 CD8a BV750 (clone 53-6.7), 1:100 CD8a V500 (clone 53-6.7), 1:400 CD95 BV605 (clone Jo2), 1:100 FR4 BUV661 (clone 12A5), 1:100 CD45.1 BUV395 (clone A20, all BD Biosciences), 1:200 CD138 BV421 (clone 281-2), 1:400 GL7 FITC (clone GL-7), 1:600 IgD PerCP-Cy5.5 (clone 11-26c2a), 1:100 CD44 BV570 (clone IM7), 1:100 CD44 BV785 (clone IM7), 1:100 CD62L PE-Fire 810 (clone W18021D), 1:100 PD-1 APC-Fire 810 (29F.1A12), 1:100 SLAM BV785 (clone TC15-12F12.2), 1:100 SLAMF6 Pacific Blue (clone 330-AJ), 1:100 CD3 PE-Fire 700 (17A2), 1:50 CXCR5 BV711 (clone L138D7), 1:50 CXCR3 BV605 (clone CXCR3-173), 1:200 ICOS PE-Cy7 (clone C398.4A, all BioLegend), 1:200 TACI APC (clone ebio8F10-3, eBioscience), 1:800 CD19 BUV661 (clone ebio1D3, Invitrogen), and APC-conjugated E7 tetramer (E7(49-57) RAHYNIVTF in $H\text{-}2D^{b}$, produced in house). Dead cells were excluded using 1:500 Zombie UV fixable viability dye (BioLegend) or 1:1000 LIVE/DEAD NIR fixable viability dye (Invitrogen).

For intracellular staining of T cell-related markers, cells were fixed with the Foxp3/Transcription factor staining kit (eBioscience). For intracellular staining of B cell-related markers, cells were

fixed with BD Cytofix/Cytoperm (BD Biosciences). In both cases, fixation was performed for 30 min on ice. After fixation, cells were either permeabilized and intracellularly stained directly or washed with FACS buffer and frozen gradually at -80°C in 10% DMSO and 90% FBS. Upon thawing, cells were washed with FACS buffer and re-fixed for 5 min at room temperature prior to permeabilization and intracellular antibody staining. The following mAbs were used: 1:50 BCL6 BUV737 (clone K112-91), 1:50 GATA3 BUV395 (clone L50-823), 1:100 RORγt BV480 (clone Q31-378, all BD Biosciences), 1:100 TCF1 Alexa fluor 488 (clone C63D9, Cell Signalling Technology), 1:200 T-bet eFluor 660 (clone ebio4B10, eBioscience) and 1:100 FOXP3 PE-Cy5 (clone FJK16s, Invitrogen). Data were acquired using a Cytek Aurora Spectral Flow Cytometer equipped with 355 nm, 405 nm, 488 nm, 561 nm and 640 nm lasers (Cytek Biosciences), and analysed with OMIQ (Dotmatics version 2024.07) or FlowJo software (TreeStar, version 10.8.1).

UMAP analysis and Wishbone trajectory analysis were performed using OMIQ on a maximum of 1000 PADRE^{+} CD4^{+} T cells per mouse (N=5/time point, total 27867 cells). For dimension reduction and Wishbone analysis, the following markers were included: PSGL1, FR4, BCL6, SLAMF6, CD44, CXCR5, SLAM, TCF1, CD62L, T-bet and PD-1. For Wishbone analysis, diffusion maps were generated first and then Wishbone was performed from diffusion components, with naive (CD62L^{low} CD44^{hi} PD-1^{-} SLAMF6^{-}) cells selected as starting point.

Preparations for transcriptome analysis

Mice received MHC-II vaccine and cells were harvested at day 5 or 10 after the first vaccination. Single cell suspensions of dLNs from 3 mice per time point were pooled to reduce biological variability. Samples were incubated with 1:50 anti-mouse CD16/32 mAb (Fc Block™, clone 2.4G2, BD Biosciences) in BD Stain buffer (with FBS, BD Biosciences) for 5 min on ice and subsequently stained with the following mAbs in BD stain buffer: 1:100 CD3 BV421 (clone 17A2, Biolegend), 1:100 CD19 PerCP-Vio700 (clone REA749, Miltenyi Biotech), 1:100 CD44 PE-Cy7 (clone IM7, eBioscience), 1:100 CD62L FITC (clone Mel-14, eBioscience) and 1:1000 LIVE/DEAD Fixable Near-IR dye (Invitrogen). CD3^{+} CD44^{hi} CD62L^{low} cells were FACS-sorted on a FACSAria II (BD Biosciences). Subsequently, samples were stained with unique hashtag oligonucleotide (HTO)-conjugated antibodies to CD45/MHC-I (TotalSeq C hashtags, C0301 to C0307 and C0309, BioLegend). Staining was performed according to the manufacturer's instructions. Briefly, FACS-sorted T cells were stained with 0.5 µg TotalSeq hashtag per sample for 30 min on ice and washed 5 times with PBS + 0.04% BSA. Prior to last wash, cells were passed through a 40 µm Flowmi Cell Strainer (Sigma-Aldrich) and samples were pooled. scRNAseq libraries were created according to the manufacturer's protocol, using a 10X Chromium single cell 5'v2 chemistry kit (10X Genomics). TCRseq library was prepared using a 10X Chromium single cell V(D)J enrichment kit for mouse T cells (10X Genomics). Nucleotide sequencing was performed on a NovaSeq6000 system (Illumina). In total, 25132 cells were analyzed for sequencing with a median sequencing-depth of 11196 reads per cell.

Processing, integration and clustering of transcriptome data

Analysis of scRNAseq and TCRseq data was performed using CellRanger (10X Genomics, v6.0.1) and Seurat (v4.3.0) in R (v4.2.3). scRNAseq reads were aligned to the mouse reference genome mm10, and barcode counting was performed using 'cellranger count'. TCRseq reads were aligned to the mouse reference genome mm10 and consensus TCR sequences were determined using 'cellranger vdj'. From the gene expression count matrix, TCR and BCR genes were removed using the 'grep' function in R with the patterns "^Tr[abgd][cvdj]" and "Ig[hkl][cvdj]" respectively. After this, the dataset was analyzed in R using the standard Seurat pipeline. Seurat object was created using 'CreateSeuratObject,' with a minimum of 200 features per cell and 3 cells expressing each gene. HTO sequencing data was added as a separate assay to the Seurat object using 'CreateAssayObject' and HTO counts were normalized by CLR method using 'NormalizeData.' HTO demultiplexing was performed using 'HTODemux' with a positive quantile of 0.99. As a result of this, each cell in the dataset was assigned to a global (singlet, doublet, or negative) and a sample-related HTO classification. Heatmap was created of HTO demultiplexing result using 'HTOHeatmap.' Singlets were selected using 'subset', and gene expression data was normalized using 'NormalizeData'. Variable features were determined using 'FindVariableFeatures' with the selection method 'mean.var.plot'. Data was scaled using 'ScaleData' on variable features. Percentage of mitochondrial gene expression per cell was determined using 'PercentageFeatureSet' with the pattern "^mt-". Singlets were filtered on number of RNA features (between 400 and 5000), number of RNA counts (<25000) and mitochondrial gene expression (<10%). Cell cycle scores for G2/M and S phase were assigned using 'CellCycleScoring', based on expression of G2/M and S phase genes. Data was normalized using 'NormalizeData' with normalization method 'LogNormalize', scale factor 25000. Top 2000 variable features were determined using 'FindVariableFeatures' with the selection method 'vst'. Data was scaled using 'ScaleData', whereby G2M scores, S scores and percentage of mitochondrial gene expression were regressed out. Principal component analysis (PCA) was run using 'RunPCA' on variable features. Clustering was performed on first 20 principal components (PCs) using 'FindNeighbors' and 'FindClusters'. Clustering resolution was set to 0.5. Uniform manifold approximation and projection (UMAP) visualization was performed using 'RunUMAP' on the first 20 PCs. Expression of known marker genes was visualized per cluster and within the UMAP projection using 'Dotplot', 'VlnPlot' and 'FeaturePlot' functions. Clusters with contaminating B cells (expression of *Cd19*, *Ms4a1*), APCs (expression of *Cd40*, *Cd274*, *Cd80*, *Cd86*) and low-quality cells (high percentage mitochondrial genes, low RNA counts) were removed. The pipeline was run again on filtered T cells, including determining variable features, data scaling, PCA, clustering and UMAP visualization. $CD4^+$ T-cell clusters were selected by expression of *Cd4*, in absence of expression of *Cd8a* and *Cd8b1* or TCRg/d. Within $CD4^+$ T-cell subsets, Help d5 and Help d10 were selected for further analysis. Clusters were annotated based on differentially expressed genes (Table S1). Venn Diagrams were created with http://bioinformatics.psb.ugent.be/webtools/Venn/.

Previously generated scRNAseq datasets from I-A^b-LCMV-gp66 tetramer-sorted CD4$^+$ T cells from LCMV-Armstrong or LCMV-Clone 13 derived at day 8 and day 21 post infection were obtained from Xia *et al.*[54]. Feature barcode matrices derived from 10x scRNA expression libraries reads aligned to mouse genome assembly GRCm38 were imported into R (version 4.4.0). A Seurat-based (version 5.2.1) quality control on the scRNA-seq samples was performed individually. TCR and BCR counts were removed from the raw gene expression count matrix (UMI) to prevent TCR/BCR chain driven clustering bias. A per-sample Seurat object was created by selecting cells on the criterium of containing a minimum of 200 genes and genes on being expressed in a minimum of 3 cells. Cells (~30%) were excluded from the subsequent analysis based on the mitochondrial content (>5%), RNA count (<1000 and >25000) and genetic content (<400 and >4000). The top 2000 highly variable genes were selected using 'FindVariableFeatures' for subsequent analysis. Cells of all 19 samples were first normalized using Seurat's 'NormalizeData' function and then scaled individually while regressing out mitochondrial gene expression and cell cycle scores for G2/M and S phase genes assigned using 'CellCycleScoring' as described above. Clustering was done on the first 30 principal components (PCs) with the default cluster resolution. Doublets were removed using 'DoubletFinder' based on the first 40 principal components (PCs).

Singlets of each sample were integrated by identifying anchors between datasets, using the top 2000 variable genes, 30 reciprocal PCA dimensions and an integration strength of 5. Clusters with contaminating B cells (expression of Cd19 Ms4a1), CD8 T cells (expression of Cd8a, Cd8b), APCs (expression of Cd40, Cd80, Cd86) or low-quality cells were removed. Data scaling and PCA was done once more on the integrated and filtered object. A k-nearest neighbors' graph was generated with the first 20 PCs and community detection for cluster identification was performed using the Louvain algorithm with a resolution of 0.4. The integrated matrix visualized as an UMAP was subsequently divided based on the day of infection (Day 8 or Day 21) and the viral strain (LCMV-Arm and LCMV-cl.13) as annotated in the metadata of the Seurat object.

Clusters were annotated based on differentially expressed genes (Table S2). To facilitate cluster identification, we compared each cluster to CD4$^+$ T-cell-specific signatures derived from vaccine-induced Th1, Tfh, and Th1/Tfh precursor populations characterized in this study. Module scores for each gene signature were calculated per cell using Seurat's 'AddModuleScore' function, based on normalized expression values from the 'data' slot of the integrated object, which were not corrected for cell cycle gene expression. Cluster-defining markers were then selected and their relative normalized expression values represented in z-scores were visualized in a heatmap using Seurat's 'pheatmap'.

The correlation plots were generated by extraction of the upregulated differentially expressed (DE) genes (only.pos = TRUE) of the concerning clusters compared to all other clusters present in the UMAP using 'FindAllMarkers' on the integrated Seurat object. Only significant DE genes (FDR < 0.05) were then used to determine the intersected (intersect) and unified (union) gene

collection when comparing the LCMV with the vaccination model. List of differentially expressed genes of LCMV-specific Th1/Tfh precursor and LCMV-specific memory-precursor cell cluster are provided in Table S3. The DE gene collection was then projected (filter and select) onto the ranked normalized expression list of all genes present in the concerning clusters. The extracted expression values of DE markers for both the LCMV and the vaccination model were correlated using the stats::cor() function and the "spearman" method for correlation. Plots were generated using ggplot() and the linear model ("lm") method to create a regression line for visualization.

The stem-like $CD4^+$ T-cell signature was derived from Cardenas *et al.*[49] (62 genes). The Th1/Tfh precursor gene signature for malaria-specific $CD4^+$ T cells was obtained from Lönnberg *et al.*[4] and comprised 1,625 dynamic genes [D statistic >50; kindly analyzed by Dr. Valentine Svensson (Tahoe Therapeutics)]. These genes were selected based on peak expression between pseudotime values of 0.5 and 1.6, corresponding to the period immediately before and after the Th1/Tfh bifurcation, which was inferred at a pseudotime value of 1.27. Gene signatures of malaria-induced Th1/Tfh precursor is provided in Table S4. A ranked list of genes and normalized expression values (ranking metric) of the vaccine-induced Th1/Tfh precursor cluster was extracted from the integrated Seurat object. The running-sum statistic was then calculated using the clusterProfiler::GSEA() function and the results were plotted with enrichplot::gseaplot2().

Statistics

For mouse experiments, statistical analysis was performed with GraphPad Prism 9.3.1 (Dotmatics) using two-tailed unpaired Student's *t*-test when comparing two groups, One-Way ANOVA with Dunnett's *post hoc* test to correct for multiple testing when comparing multiple groups at one timepoint or Two-Way ANOVA with Šidák *post hoc* test to correct for multiple testing when comparing multiple groups at multiple time points. Explanation of statistical parameters such as mean, SD and n are mentioned in figure legends. P values < 0.05 were considered statistically significant. Statistics were denoted as follows: * P≤0.05, ** P≤0.01, *** P≤0.001, and **** P≤0.0001. Plots were generated with ggplot2 (3.3.3) and GraphPad Prism 9.3.1.

Data availability

All data generated and analyzed in this study are included in this article, its supplementary information, or have been made available in public repositories. ScRNAseq and TCRseq data generated in this study are available from the NCBI Gene Expression Omnibus (GEO) repository under the accession code GSE249046. scRNAseq data of GP66 tet^+ $CD4^+$ T cells following LCMV-Armstrong or LCMV-Clone 13 infections were extracted and re-analysed from GSE181474[54]. scRNAseq data of *Plasmodium*-specific TCR transgenic $CD4^+$ T (PbTII) cells post *Plasmodium chabaudi chabaudi* AS (PcAS) infection were extracted and re-analysed from Lönnberg et al.

2017[4]. Gene signature of stem-like CD4$^+$ T cells was extracted from Cardenas et al. 2024[50]. Flow cytometry data from this study are available upon request.

Acknowledgements

We thank the Animal facility, Flow Cytometry Facility and Leiden Genome Technology Center from the LUMC for technical assistance. We also thank Dr. Vincent van Unen (LUMC) for his support with scRNAseq data analysis, and Dr. Tapio Lönnberg (University of Turku) and Dr. Valentine Svensson (Tahoe Therapeutics) for providing us with the malaria-induced Th1/Tfh gene signature. This work was supported by grants 11079 (to J.Bo and Y.X) and 10894 (to J.Bo) from the Dutch Cancer Society (KWF); a grant from Oncode to J.Bo; a VENI grant (ZonMw project n. 09150162010046) from the Dutch Science Foundation (NWO) and a Gisela Thier fellowship from Leiden University Medical Center to F.S.

Author contributions

Conceptualization: D.M.T.B, J.Bo, F.S. Methodology and investigation: D.M.T.B, J.Bu, M.D.S, M.R, X.L, T.d.W, Y.X, F.S. Formal analysis, visualization and data curation: D.M.T.B, J.Bu, M.d.K, F.S. Writing - original draft: D.M.T.B, J.Bo, F.S. Writing - review and editing: D.M.T.B, J.Bu, M.D.S, M.R, M.d.K, X.L, T.d.W, Y.X, J.Bo, F.S. Project administration, funding acquisition and supervision: J.Bo. and F.S.

Competing Interests

The authors declare no competing interests.

References

1. Yin, X., Chen, S., and Eisenbarth, S.C. (2021). Dendritic Cell Regulation of T Helper Cells. Annual review of immunology *39*, 759-790. 10.1146/ANNUREV-IMMUNOL-101819-025146.
2. Vinuesa, C.G., Linterman, M.A., Yu, D., and Maclennan, I.C.M. (2016). Follicular Helper T Cells. Annual review of immunology *34*, 335-368. 10.1146/ANNUREV-IMMUNOL-041015-055605.
3. Osum, K.C., and Jenkins, M.K. (2023). Toward a general model of CD4+ T cell subset specification and memory cell formation. Immunity *56*, 475-484. 10.1016/J.IMMUNI.2023.02.010.
4. Lönnberg, T., Svensson, V., James, K.R., Fernandez-Ruiz, D., Sebina, I., Montandon, R., Soon, M.S.F., Fogg, L.G., Nair, A.S., Liligeto, U.N., et al. (2017). Single-cell RNA-seq and computational analysis using temporal mixture modelling resolves Th1/Tfh fate bifurcation in malaria. Science immunology *2*. 10.1126/SCIIMMUNOL.AAL2192.
5. Duckworth, B.C., and Groom, J.R. (2021). Conversations that count: Cellular interactions that drive T cell fate. Immunological reviews *300*, 203-219. 10.1111/IMR.12945.
6. Eisenbarth, S.C., Baumjohann, D., Craft, J., Fazilleau, N., Ma, C.S., Tangye, S.G., Vinuesa, C.G., and Linterman, M.A. (2021). CD4+ T cells that help B cells - a proposal for uniform nomenclature. Trends in immunology *42*, 658-669. 10.1016/J.IT.2021.06.003.
7. Künzli, M., and Masopust, D. (2023). CD4+ T cell memory. Nature Immunology 2023 *24*, 1-12. 10.1038/s41590-023-01510-4.
8. Dalit, L., Tan, C.W., Sheikh, A.A., Munnings, R., Howson, L.J., Alvarado, C., Hussain, T., Zaini, A., Cooper, L., Kirn, A., et al. (2025). Divergent cytokine and transcriptional signatures control functional T follicular helper cell heterogeneity. Nature immunology *26*, 1821-1835. 10.1038/S41590-025-02258-9.
9. Dudziak, D., Kamphorst, A.O., Heidkamp, G.F., Buchholz, V.R., Trumpfheller, C., Yamazaki, S., Cheong, C., Liu, K., Lee, H.W., Chae, G.P., et al. (2007). Differential antigen processing by dendritic cell subsets in vivo. Science *315*, 107-111. 10.1126/science.1136080
10. De Giovanni, M., Cutillo, V., Giladi, A., Sala, E., Maganuco, C.G., Medaglia, C., Di Lucia, P., Bono, E., Cristofani, C., Consolo, E., et al. (2020). Spatiotemporal regulation of type I interferon expression determines the antiviral polarization of CD4+ T cells. Nature Immunology *21*, 321-330. 10.1038/s41590-020-0596-6.
11. Hilligan, K.L., and Ronchese, F. (2020). Antigen presentation by dendritic cells and their instruction of CD4+ T helper cell responses. Cellular & Molecular Immunology 2020 17:6 *17*, 587-599. 10.1038/s41423-020-0465-0.
12. Den Haan, J.M.M., Lehar, S.M., and Bevan, M.J. (2000). CD8(+) but not CD8(-) dendritic cells cross-prime cytotoxic T cells in vivo. The Journal of experimental medicine *192*, 1685-1695. 10.1084/JEM.192.12.1685.
13. Hildner, K., Edelson, B.T., Purtha, W.E., Diamond, M., Matsushita, H., Kohyama, M., Calderon, B., Schraml, B.U., Unanue, E.R., Diamond, M.S., et al. (2008). Batf3 deficiency reveals a critical role for CD8alpha+ dendritic cells in cytotoxic T cell immunity. Science (New York, N.Y.) *322*, 1097-1100. 10.1126/SCIENCE.1164206.
14. Martínez-López, M., Iborra, S., Conde-Garrosa, R., and Sancho, D. (2015). Batf3-dependent CD103+ dendritic cells are major producers of IL-12 that drive local Th1 immunity against Leishmania major infection in mice. European journal of immunology *45*, 119-129. 10.1002/EJI.201444651.
15. Ferris, S.T., Durai, V., Wu, R., Theisen, D.J., Ward, J.P., Bern, M.D., Davidson, J.T., Bagadia, P., Liu, T., Briseño, C.G., et al. (2020). cDC1 prime and are licensed by CD4+ T cells to induce anti-tumour immunity. Nature *584*, 624-629. 10.1038/S41586-020-2611-3.

16. Wu, R., and Murphy, K.M. (2022). DCs at the center of help: Origins and evolution of the three-cell-type hypothesis. The Journal of experimental medicine *219*. 10.1084/JEM.20211519.

17. Borst, J., Ahrends, T., Bąbała, N., Melief, C.J.M., and Kastenmüller, W. (2018). CD4+ T cell help in cancer immunology and immunotherapy. Nature Reviews Immunology. 18(10):635-647.

18. Lei, X., de Groot, D.C., Welters, M.J.P., de Wit, T., Schrama, E., van Eenennaam, H., Santegoets, S.J., Oosenbrug, T., van der Veen, A., Vos, J.L., et al. (2024). CD4+ T cells produce IFN-I to license cDC1s for induction of cytotoxic T-cell activity in human tumors. Cellular & molecular immunology *21*, 374-392. 10.1038/S41423-024-01133-1.

19. Crotty, S. (2014). T follicular helper cell differentiation, function, and roles in disease. Immunity *41*, 529-542. 10.1016/J.IMMUNI.2014.10.004.

20. Nakayamada, S., Kanno, Y., Takahashi, H., Jankovic, D., Lu, K.T., Johnson, T.A., Sun, H.w., Vahedi, G., Hakim, O., Handon, R., et al. (2011). Early Th1 Cell Differentiation Is Marked by a Tfh Cell-like Transition. Immunity *35*, 919-931. 10.1016/J.IMMUNI.2011.11.012.

21. Choi, J., Diao, H., Faliti, C.E., Truong, J., Rossi, M., Bélanger, S., Yu, B., Goldrath, A.W., Pipkin, M.E., and Crotty, S. (2020). Bcl-6 is the nexus transcription factor of T follicular helper cells via repressor-of-repressor circuits. Nature immunology *21*, 777-789. 10.1038/S41590-020-0706-5.

22. Nurieva, R.I., Chung, Y., Martinez, G.J., Yang, X.O., Tanaka, S., Matskevitch, T.D., Wang, Y.H., and Dong, C. (2009). Bcl6 mediates the development of T follicular helper cells. Science (New York, N.Y.) *325*, 1001-1005. 10.1126/SCIENCE.1176676.

23. Johnston, R.J., Poholek, A.C., DiToro, D., Yusuf, I., Eto, D., Barnett, B., Dent, A.L., Craft, J., and Crotty, S. (2009). Bcl6 and Blimp-1 are reciprocal and antagonistic regulators of T follicular helper cell differentiation. Science (New York, N.Y.) *325*, 1006-1010. 10.1126/SCIENCE.1175870.

24. Oestreich, K.J., Mohn, S.E., and Weinmann, A.S. (2012). Molecular mechanisms that control the expression and activity of Bcl-6 in TH1 cells to regulate flexibility with a TFH-like gene profile. Nature Immunology 2012 13:4 *13*, 405-411. 10.1038/ni.2242.

25. Fang, D., Cui, K., Mao, K., Hu, G., Li, R., Zheng, M., Riteau, N., Reiner, S.L., Sher, A., Zhao, K., and Zhu, J. (2018). Transient T-bet expression functionally specifies a distinct T follicular helper subset. Journal of Experimental Medicine *215*, 2705-2714. 10.1084/JEM.20180927.

26. Weinstein, J.S., Laidlaw, B.J., Lu, Y., Wang, J.K., Schulz, V.P., Li, N., Herman, E.I., Kaech, S.M., Gallagher, P.G., and Craft, J. (2018). STAT4 and T-bet control follicular helper T cell development in viral infections. Journal of Experimental Medicine *215*, 337-355. 10.1084/JEM.20170457.

27. Cho, Y.L., Flossdorf, M., Kretschmer, L., Höfer, T., Busch, D.H., and Buchholz, V.R. (2017). TCR Signal Quality Modulates Fate Decisions of Single CD4+ T Cells in a Probabilistic Manner. Cell Reports *20*, 806-818. 10.1016/J.CELREP.2017.07.005.

28. Fazilleau, N., McHeyzer-Williams, L.J., Rosen, H., and McHeyzer-Williams, M.G. (2009). The function of follicular helper T cells is regulated by the strength of T cell antigen receptor binding. Nature immunology *10*, 375-384. 10.1038/NI.1704.

29. Tubo, N.J., Pagán, A.J., Taylor, J.J., Nelson, R.W., Linehan, J.L., Ertelt, J.M., Huseby, E.S., Way, S.S., and Jenkins, M.K. (2013). Single Naive CD4+ T Cells from a Diverse Repertoire Produce Different Effector Cell Types during Infection. Cell *153*, 785-796. 10.1016/J.CELL.2013.04.007.

30. Künzli, M., Reuther, P., Pinschewer, D.D., and King, C.G. (2021). Opposing effects of T cell receptor signal strength on CD4 T cells responding to acute versus chronic viral infection. eLife *10*. 10.7554/ELIFE.61869.

31. Alterauge, D., Bagnoli, J.W., Dahlström, F., Bradford, B.M., Mabbott, N.A., Buch, T., Enard, W., and Baumjohann, D. (2020). Continued Bcl6 Expression Prevents the Transdifferentiation of Established Tfh Cells into Th1 Cells during Acute Viral Infection. Cell Reports *33*, 108232-108232. 10.1016/J.CELREP.2020.108232.

32. O'Shea, J., and Paul, W.E. (2010). Mechanisms underlying lineage commitment and plasticity of helper CD4+ T cells. Science (New York, N.Y.) *327*, 1098-1102. 10.1126/SCIENCE.1178334.

33. Kiner, E., Willie, E., Vijaykumar, B., Chowdhary, K., Schmutz, H., Chandler, J., Schnell, A., Thakore, P.I., LeGros, G., Mostafavi, S., et al. (2021). Gut CD4+ T cell phenotypes are a continuum molded by microbes, not by TH archetypes. Nature immunology *22*, 216-228. 10.1038/S41590-020-00836-7.

34. Ahrends, T., Babała, N., Xiao, Y., Yagita, H., Van Eenennaam, H., and Borst, J. (2016). CD27 Agonism Plus PD-1 Blockade Recapitulates CD4 + T-cell Help in Therapeutic Anticancer Vaccination. Cancer Research *76*, 2921-2931. 10.1158/0008-5472.CAN-15-3130.

35. Ahrends, T., Busselaar, J., Severson, T.M., Bąbała, N., de Vries, E., Bovens, A., Wessels, L., van Leeuwen, F., and Borst, J. (2019). CD4+ T cell help creates memory CD8+ T cells with innate and help-independent recall capacities. Nature communications *10*. 10.1038/S41467-019-13438-1.

36. **3**Ahrends, T., Spanjaard, A., Pilzecker, B., Bąbała, N., Bovens, A., Xiao, Y., Jacobs, H., and Borst, J. (2017). CD4+ T Cell Help Confers a Cytotoxic T Cell Effector Program Including Coinhibitory Receptor Downregulation and Increased Tissue Invasiveness. Immunity *47*, 848-861.e845. 10.1016/J.IMMUNI.2017.10.009.

37. Oosterhuis, K., Aleyd, E., Vrijland, K., Schumacher, T.N., and Haanen, J.B. (2012). Rational Design of DNA Vaccines for the Induction of Human Papillomavirus Type 16 E6- and E7-Specific Cytotoxic T-Cell Responses. Human Gene Therapy *23*, 1301-1312. 10.1089/hum.2012.101.

38. Alexander, J., Sidney, J., Southwood, S., Ruppert, J., Oseroff, C., Maewal, A., Snoke, K., Serra, H.M., Kubo, R.T., Sette, A., and Grey, H.M. (1994). Development of high potency universal DR-restricted helper epitopes by modification of high affinity DR-blocking peptides. Immunity *1*, 751-761. 10.1016/S1074-7613(94)80017-0.

39. Rice, J., Elliott, T., Buchan, S., and Stevenson, F.K. (2001). DNA fusion vaccine designed to induce cytotoxic T cell responses against defined peptide motifs: implications for cancer vaccines. Journal of immunology (Baltimore, Md. : 1950) *167*, 1558-1565. 10.4049/JIMMUNOL.167.3.1558.

40. Bosma, D.M.T., Busselaar, J., Staal, M.D., Frijlink, E., Mack, M., Salerno, F., and Borst, J. (2025). CD4+ T-cell help delivery to monocyte-derived dendritic cells promotes effector differentiation of helper and cytotoxic T cells. Immunology letters *275*. 10.1016/J.IMLET.2025.107022.

41. Babała, N., Bovens, A., De Vries, E., Iglesias-Guimarais, V., Ahrends, T., Krummel, M.F., Borst, J., and Bins, A.D. (2018). Subcellular localization of antigen in keratinocytes dictates delivery of CD4 þ T-cell Help for the CTL response upon therapeutic DNA vaccination into the Skin. Cancer Immunology Research *6*, 835-847. 10.1158/2326-6066.CIR-17-0408.

42. Bins, A.D., Jorritsma, A., Wolkers, M.C., Hung, C.F., Wu, T.C., Schumacher, T.N.M., and Haanen, J.B.A.G. (2005). A rapid and potent DNA vaccination strategy defined by in vivo monitoring of antigen expression. Nature medicine *11*, 899-904. 10.1038/NM1264.

43. Marshall, H.D., Chandele, A., Jung, Y.W., Meng, H., Poholek, A.C., Parish, I.A., Rutishauser, R., Cui, W., Kleinstein, S.H., Craft, J., and Kaech, S.M. (2011). Differential Expression of Ly6C and T-bet Distinguish Effector and Memory Th1 CD4+ Cell Properties during Viral Infection. Immunity *35*, 633-646. 10.1016/J.IMMUNI.2011.08.016.

44. Shaw, L.A., Bélanger, S., Omilusik, K.D., Cho, S., Scott-Browne, J.P., Nance, J.P., Goulding, J., Lasorella, A., Lu, L.F., Crotty, S., and Goldrath, A.W. (2016). Id2 reinforces TH1 differentiation and inhibits E2A to repress TFH differentiation. Nature immunology *17*, 834-843. 10.1038/NI.3461.

45. Zou, D., Yin, Z., Yi, S.G., Wang, G., Guo, Y., Xiao, X., Li, S., Zhang, X., Gonzalez, N.M., Minze, L.J., et al. (2024). CD4+ T cell immunity is dependent on an intrinsic stem-like program. Nature immunology *25*, 66-76. 10.1038/S41590-023-01682-Z.

46. Choi, Y.S., Gullicksrud, J.A., Xing, S., Zeng, Z., Shan, Q., Li, F., Love, P.E., Peng, W., Xue, H.H., and Crotty, S. (2015). LEF-1 and TCF-1 orchestrate TFH differentiation by regulating differentiation circuits upstream of the transcriptional repressor Bcl6. Nature Immunology 2015 16:9 *16*, 980-990. 10.1038/ni.3226.

47. Setty, M., Tadmor, M.D., Reich-Zeliger, S., Angel, O., Salame, T.M., Kathail, P., Choi, K., Bendall, S., Friedman, N., and Pe'Er, D. (2016). Wishbone identifies bifurcating developmental trajectories from single-cell data. Nature biotechnology *34*, 637-645. 10.1038/NBT.3569.

48. Busselaar, J., Tian, S., van Eenennaam, H., and Borst, J. (2020). Helpless Priming Sends CD8+ T Cells on the Road to Exhaustion. Frontiers in Immunology *11*, 2637-2637. 10.3389/fimmu.2020.592569.

49. Cardenas, M.A., Prokhnevska, N., Sobierajska, E., Gregorova, P., Medina, C.B., Valanparambil, R.M., Greenwald, R., DelBalzo, L., Bilen, M.A., Joshi, S.S., et al. (2024). Differentiation fate of a stem-like CD4 T cell controls immunity to cancer. Nature 2024 636:8041 *636*, 224-232. 10.1038/s41586-024-08076-7.

50. Agata, Y., Kawasaki, A., Nishimura, H., Ishida, Y., Tsubata, T., Yagita, H., and Honjo, T. (1996). Expression of the PD-1 antigen on the surface of stimulated mouse T and B lymphocytes. International immunology *8*, 765-772. 10.1093/INTIMM/8.5.765.

51. Baumeister, S.H., Freeman, G.J., Dranoff, G., and Sharpe, A.H. (2016). Coinhibitory Pathways in Immunotherapy for Cancer. Annual review of immunology *34*, 539-573. 10.1146/ANNUREV-IMMUNOL-032414-112049.

52. Cibrián, D., and Sánchez-Madrid, F. (2017). CD69: from activation marker to metabolic gatekeeper. European journal of immunology *47*, 946-953. 10.1002/EJI.201646837.

53. Simms, P.E., and Ellis, T.M. (1996). Utility of flow cytometric detection of CD69 expression as a rapid method for determining poly- and oligoclonal lymphocyte activation. Clinical and diagnostic laboratory immunology *3*, 301-304. 10.1128/CDLI.3.3.301-304.1996.

54. Xia, Y., Sandor, K., Pai, J.A., Daniel, B., Raju, S., Wu, R., Hsiung, S., Qi, Y., Yangdon, T., Okamoto, M., et al. (2022). BCL6-dependent TCF-1+ progenitor cells maintain effector and helper CD4+ T cell responses to persistent antigen. Immunity *55*, 1200-1215.e1206. 10.1016/J.IMMUNI.2022.05.003.

55. Nguyen, C., Kudek, M., Zander, R., Niu, H., Shen, J., Bauer, A., Alson, D., Khatun, A., Chen, Y., Sun, J., et al. (2024). Bhlhe40 Promotes CD4+ T Helper 1 Cell and Suppresses T Follicular Helper Cell Differentiation during Viral Infection. Journal of immunology (Baltimore, Md. : 1950) *212*, 1829-1842. 10.4049/JIMMUNOL.2300355.

56. Xu, W., Zhao, X., Wang, X., Feng, H., Gou, M., Jin, W., Wang, X., Liu, X., and Dong, C. (2019). The Transcription Factor Tox2 Drives T Follicular Helper Cell Development via Regulating Chromatin Accessibility. Immunity *51*, 826-839.e825. 10.1016/J.IMMUNI.2019.10.006.

57. Baumjohann, D., Okada, T., and Ansel, K.M. (2011). Cutting Edge: Distinct Waves of BCL6 Expression during T Follicular Helper Cell Development. The Journal of Immunology *187*, 2089-2092. 10.4049/JIMMUNOL.1101393.

58. Choi, Y.S., Kageyama, R., Eto, D., Escobar, T.C., Johnston, R.J., Monticelli, L., Lao, C., and Crotty, S. (2011). ICOS Receptor Instructs T Follicular Helper Cell versus Effector Cell Differentiation via Induction of the Transcriptional Repressor Bcl6. Immunity *34*, 932-946. 10.1016/J.IMMUNI.2011.03.023.

59. Ma, C.S., Deenick, E.K., Batten, M., and Tangye, S.G. (2012). The origins, function, and regulation of T follicular helper cells. The Journal of Experimental Medicine *209*, 1241-1241. 10.1084/JEM.20120994.

60. Ditoro, D., Winstead, C., Pham, D., Witte, S., Andargachew, R., Singer, J.R., Wilson, C.G., Zindl, C.L., Luther, R.J., Silberger, D.J., et al. (2018). Differential IL-2 expression defines developmental fates of follicular versus nonfollicular helper T cells. Science *361*. 10.1126/SCIENCE.AAO2933.

61. Schorer, M., Kuchroo, V.K., and Joller, N. (2019). Role of co-stimulatory molecules in T helper cell differentiation. Advances in Experimental Medicine and Biology *1189*, 153-177. 10.1007/978-981-32-9717-3_6.

62. Linterman, M.A., Denton, A.E., Divekar, D.P., Zvetkova, I., Kane, L., Ferreira, C., Veldhoen, M., Clare, S., Dougan, G., Espéli, M., and Smith, K.G.C. (2014). CD28 expression is required after T cell priming for helper T cell responses and protective immunity to infection. eLife *3*, 1-21. 10.7554/ELIFE.03180.

63. Acuto, O., and Michel, F. (2003). CD28-mediated co-stimulation: a quantitative support for TCR signalling. Nature reviews. Immunology *3*, 939-951. 10.1038/NRI1248.

64. Collins, A.V., Brodie, D.W., Gilbert, R.J.C., Iaboni, A., Manso-Sancho, R., Walse, B., Stuart, D.I., Van Der Merwe, P.A., and Davis, S.J. (2002). The interaction properties of costimulatory molecules revisited. Immunity *17*, 201-210. 10.1016/S1074-7613(02)00362-X.

65. Wang, C.J., Heuts, F., Ovcinnikovs, V., Wardzinski, L., Bowers, C., Schmidt, E.M., Kogimtzis, A., Kenefeck, R., Sansom, D.M., Walker, L.S.K., and Weiss, A. (2015). CTLA-4 controls follicular helper T-cell differentiation by regulating the strength of CD28 engagement. Proceedings of the National Academy of Sciences of the United States of America *112*, 524-529. 10.1073/PNAS.1414576112.

66. Baumjohann, D., Preite, S., Reboldi, A., Ronchi, F., Ansel, K.M., Lanzavecchia, A., and Sallusto, F. (2013). Persistent Antigen and Germinal Center B Cells Sustain T Follicular Helper Cell Responses and Phenotype. Immunity *38*, 596-605. 10.1016/J.IMMUNI.2012.11.020.

67. Grewal, I.S., Xu, J., and Flavell, R.A. (1995). Impairment of antigen-specific T-cell priming in mice lacking CD40 ligand. Nature *378*, 617-620. 10.1038/378617A0.

68. Liu, D., Xu, H., Shih, C., Wan, Z., Ma, X., Ma, W., Luo, D., and Qi, H. (2014). T–B-cell entanglement and ICOSL-driven feed-forward regulation of germinal centre reaction. Nature 2014 517:7533 *517*, 214-218. 10.1038/nature13803.

69. Shin, C., Han, J.A., Koh, H., Choi, B., Cho, Y., Jeong, H., Ra, J.S., Sung, P.S., Shin, E.C., Ryu, S., and Do, Y. (2015). CD8α– Dendritic Cells Induce Antigen-Specific T Follicular Helper Cells Generating Efficient Humoral Immune Responses. Cell Reports *11*, 1929-1940. 10.1016/J.CELREP.2015.05.042.

70. Xu, H., Li, X., Liu, D., Li, J., Zhang, X., Chen, X., Hou, S., Peng, L., Xu, C., Liu, W., et al. (2013). Follicular T-helper cell recruitment governed by bystander B cells and ICOS-driven motility. Nature *496*, 523-527. 10.1038/NATURE12058.

71. Chen, X., Ma, W., Zhang, T., Wu, L., and Qi, H. (2015). Phenotypic Tfh development promoted by CXCR5-controlled re-localization and IL-6 from radiation-resistant cells. Protein & cell *6*, 825-832. 10.1007/S13238-015-0210-0.

72. Edelson, B.T., Bradstreet, T.R., Kc, W., Hildner, K., Herzog, J.W., Sim, J., Russell, J.H., Murphy, T.L., Unanue, E.R., and Murphy, K.M. (2011). Batf3-dependent CD11b(low/-) peripheral dendritic cells are GM-CSF-independent and are not required for Th cell priming after subcutaneous immunization. PloS one *6*. 10.1371/JOURNAL.PONE.0025660.

73. McManus, D.T., Valanparambil, R.M., Medina, C.B., Scharer, C.D., McGuire, D.J., Sobierajska, E., Hu, Y., Chang, D.Y., Wieland, A., Lee, J., et al. (2025). An early precursor CD8+ T cell that adapts to acute or chronic viral infection. Nature *640*, 772-781. 10.1038/S41586-024-08562-Y.

74. Pritykin, Y., van der Veeken, J., Pine, A.R., Zhong, Y., Sahin, M., Mazutis, L., Pe'er, D., Rudensky, A.Y., and Leslie, C.S. (2021). A unified atlas of CD8 T cell dysfunctional states in cancer and infection. Molecular cell *81*, 2477-2493.e2410. 10.1016/J.MOLCEL.2021.03.045.

75. Prokhnevska, N., Cardenas, M.A., Valanparambil, R.M., Sobierajska, E., Barwick, B.G., Jansen, C., Reyes Moon, A., Gregorova, P., delBalzo, L., Greenwald, R., et al. (2023). CD8+ T cell activation in cancer comprises an initial activation phase in lymph nodes followed by effector differentiation within the tumor. Immunity *56*, 107-124.e105. 10.1016/J.IMMUNI.2022.12.002.

76. Gerner, M.Y., Casey, K.A., Kastenmuller, W., and Germain, R.N. (2017). Dendritic cell and antigen dispersal landscapes regulate T cell immunity. The Journal of experimental medicine *214*, 3105-3122. 10.1084/JEM.20170335.

77. Krishnaswamy, J.K., Gowthaman, U., Zhang, B., Mattsson, J., Szeponik, L., Liu, D., Wu, R., White, T., Calabro, S., Xu, L., et al. (2017). Migratory CD11b+ conventional dendritic cells induce T follicular helper cell-dependent antibody responses. Science immunology *2*. 10.1126/SCIIMMUNOL.AAM9169.

78. Li, J., Lu, E., Yi, T., and Cyster, J.G. (2016). EBI2 augments Tfh cell fate by promoting interaction with IL-2-quenching dendritic cells. Nature 2016 533:7601 *533*, 110-114. 10.1038/nature17947.

79. Kerfoot, S.M., Yaari, G., Patel, J.R., Johnson, K.L., Gonzalez, D.G., Kleinstein, S.H., and Haberman, A.M. (2011). Germinal center B cell and T follicular helper cell development initiates in the interfollicular zone. Immunity *34*, 947-960. 10.1016/J.IMMUNI.2011.03.024.

80. Kim, Y.J., Choi, J., and Choi, Y.S. (2024). Transcriptional regulation of Tfh dynamics and the formation of immunological synapses. Experimental & Molecular Medicine 2024 56:6 *56*, 1365-1372. 10.1038/s12276-024-01254-7.

81. Song, W., and Craft, J. (2024). T Follicular Helper Cell Heterogeneity. Annual review of immunology *42*, 127-152. 10.1146/ANNUREV-IMMUNOL-090222-102834.

82. Groom, J.R., Richmond, J., Murooka, T.T., Sorensen, E.W., Sung, J.H., Bankert, K., von Andrian, U.H., Moon, J.J., Mempel, T.R., and Luster, A.D. (2012). CXCR3 chemokine receptor-ligand interactions in the lymph node optimize CD4+ T helper 1 cell differentiation. Immunity *37*, 1091-1103. 10.1016/J.IMMUNI.2012.08.016.

83. Eickhoff, S., Brewitz, A., Gerner, M.Y., Klauschen, F., Komander, K., Hemmi, H., Garbi, N., Kaisho, T., Germain, R.N., and Kastenmüller, W. (2015). Robust Anti-viral Immunity Requires Multiple Distinct T Cell-Dendritic Cell Interactions. Cell *162*, 1322-1337. 10.1016/J.CELL.2015.08.004.

84. Hor, J.L., Whitney, P.G., Zaid, A., Brooks, A.G., Heath, W.R., and Mueller, S.N. (2015). Spatiotemporally Distinct Interactions with Dendritic Cell Subsets Facilitates CD4+ and CD8+ T Cell Activation to Localized Viral Infection. Immunity *43*, 554-565. 10.1016/J.IMMUNI.2015.07.020.

85. Morita, R., Schmitt, N., Bentebibel, S.E., Ranganathan, R., Bourdery, L., Zurawski, G., Foucat, E., Dullaers, M., Oh, S.K., Sabzghabaei, N., et al. (2011). Human Blood CXCR5+CD4+ T Cells Are Counterparts of T Follicular Cells and Contain Specific Subsets that Differentially Support Antibody Secretion. Immunity *34*, 108-121. 10.1016/J.IMMUNI.2010.12.012.

86. Bentebibel, S.E., Khurana, S., Schmitt, N., Kurup, P., Mueller, C., Obermoser, G., Palucka, A.K., Albrecht, R.A., Garcia-Sastre, A., Golding, H., and Ueno, H. (2016). ICOS+PD-1+CXCR3+ T follicular helper cells contribute to the generation of high-avidity antibodies following influenza vaccination. Scientific Reports 2016 6:1 *6*, 1-8. 10.1038/srep26494.

87. Bentebibel, S.E., Lopez, S., Obermoser, G., Schmitt, N., Mueller, C., Harrod, C., Flano, E., Mejias, A., Albrecht, R.A., Blankenship, D., et al. (2013). Induction of ICOS+CXCR3+CXCR5+ T H cells correlates with antibody responses to influenza vaccination. Science Translational Medicine *5*. 10.1126/scitranslmed.3005191

88. Martin-Gayo, E., Cronin, J., Hickman, T., Ouyang, Z., Lindqvist, M., Kolb, K.E., Schulze zur Wiesch, J., Cubas, R., Porichis, F., Shalek, A.K., et al. (2017). Circulating CXCR5+CXCR3+PD-1lo Tfh-like cells in HIV-1 controllers with neutralizing antibody breadth. JCI Insight *2*, e89574-e89574. 10.1172/JCI.INSIGHT.89574.

89. Schulz, O., Edwards, A.D., Schito, M., Aliberti, J., Manickasingham, S., Sher, A., and Reis e Sousa, C. (2000). CD40 triggering of heterodimeric IL-12 p70 production by dendritic cells in vivo requires a microbial priming signal. Immunity *13*, 453-462. 10.1016/S1074-7613(00)00045-5.

90. Wu, R., Ohara, R.A., Jo, S., Liu, T.T., Ferris, S.T., Ou, F., Kim, S., Theisen, D.J., Anderson, D.A., Wong, B.W., et al. (2022). Mechanisms of CD40-dependent cDC1 licensing beyond costimulation. Nature immunology *23*, 1536-1550. 10.1038/S41590-022-01324-W.

91. Duckworth, B.C., Lafouresse, F., Wimmer, V.C., Broomfield, B.J., Dalit, L., Alexandre, Y.O., Sheikh, A.A., Qin, R.Z., Alvarado, C., Mielke, L.A., et al. (2021). Effector and stem-like memory cell fates are imprinted in distinct lymph node niches directed by CXCR3 ligands. Nature immunology *22*, 434-448. 10.1038/S41590-021-00878-5.

92. De Koker, S., Van Hoecke, L., De Beuckelaer, A., Roose, K., Deswarte, K., Willart, M.A., Bogaert, P., Naessens, T., De Geest, B.G., Saelens, X., et al. (2017). Inflammatory monocytes regulate Th1 oriented immunity to CpG adjuvanted protein vaccines through production of IL-12. Scientific reports *7*. 10.1038/S41598-017-06236-6.

93. Leal, J.M., Huang, J.Y., Kohli, K., Stoltzfus, C., Lyons-Cohen, M.R., Olin, B.E., Gale, M., and Gerner, M.Y. (2021). Innate cell microenvironments in lymph nodes shape the generation of T cell responses during type I inflammation. Science Immunology *6*, eabb9435-eabb9435. 10.1126/sciimmunol.abb9435.

94. Sheikh, A.A., and Groom, J.R. (2021). Transcription tipping points for T follicular helper cell and T-helper 1 cell fate commitment. Cellular & molecular immunology *18*, 528-538. 10.1038/S41423-020-00554-Y.

95. Sheikh, A.A., Cooper, L., Feng, M., Souza-Fonseca-Guimaraes, F., Lafouresse, F., Duckworth, B.C., Huntington, N.D., Moon, J.J., Pellegrini, M., Nutt, S.L., et al. (2019). Context-Dependent Role for T-bet in T Follicular Helper Differentiation and Germinal Center Function following Viral Infection. Cell reports *28*, 1758-1772.e1754. 10.1016/J.CELREP.2019.07.034.

96. Zheng, L., Qin, S., Si, W., Wang, A., Xing, B., Gao, R., Ren, X., Wang, L., Wu, X., Zhang, J., et al. (2021). Pan-cancer single-cell landscape of tumor-infiltrating T cells. Science (New York, N.Y.) *374*. 10.1126/SCIENCE.ABE6474.

97. Nüssing, S., House, I.G., Kearney, C.J., Chen, A.X.Y., Vervoort, S.J., Beavis, P.A., Oliaro, J., Johnstone, R.W., Trapani, J.A., and Parish, I.A. (2020). Efficient CRISPR/Cas9 Gene Editing in Uncultured Naive Mouse T Cells for In Vivo Studies. J Immunol *204*, 2308-2315. 10.4049/jimmunol.1901396.

98. Seki, A., and Rutz, S. (2018). Optimized RNP transfection for highly efficient CRISPR/Cas9-mediated gene knockout in primary T cells. J Exp Med *215*, 985-997. 10.1084/jem.20171626.

Supplementary Figures

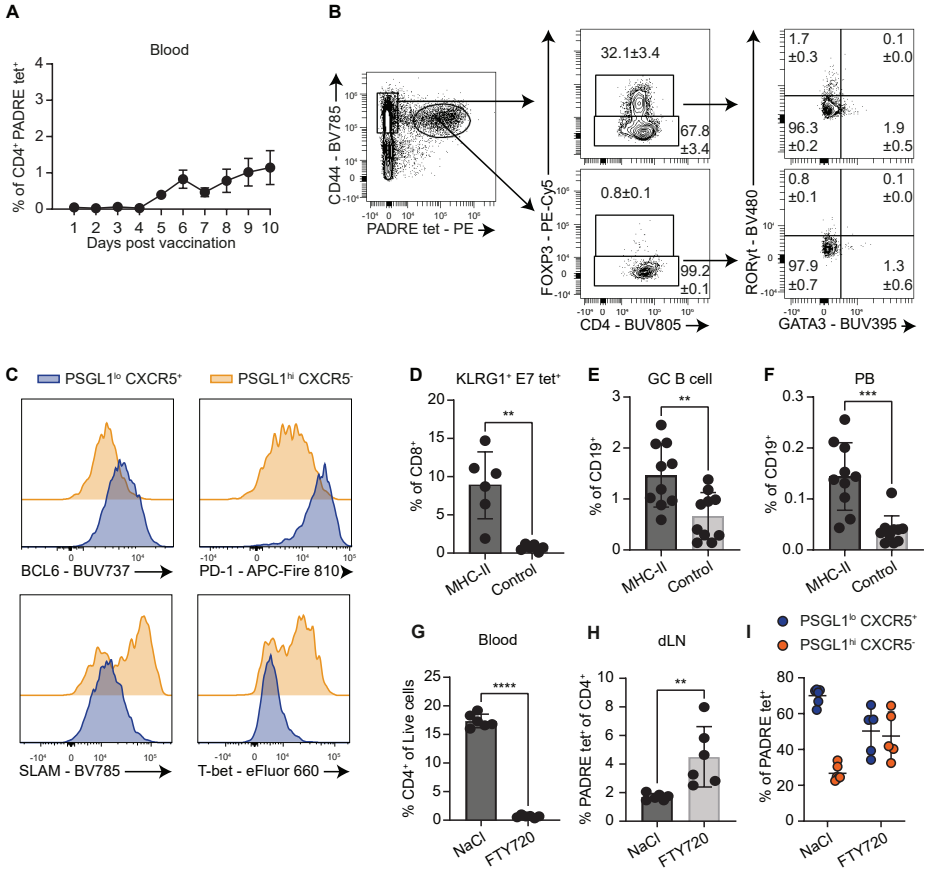

Figure S1 (related to Figure 1): A vaccination model to study differentiation of endogenous, polyclonal CD4⁺ T cells into Th1 or Tfh cells. (A) Frequency of PADRE tet⁺ CD4⁺ T cells in blood over time after vaccination (N=5 mice per group). (B) Representative contour plots depicting FOXP3, GATA3 and RORγt expression in CD44⁺ PADRE tet⁻ (top) and CD44⁺ PADRE tet⁺ (bottom) CD4⁺ T cells. (C) Representative histograms of BCL6, PD-1, SLAM, and T-bet expression in PSGL1^{lo} CXCR5⁺ (blue) and PSGL1^{hi} CXCR5⁻ (orange) CD44⁺ PADRE tet⁺ CD4⁺ T cells in dLNs at day 8 post-vaccination. (D) Frequency of antigen-specific effector CD8⁺ T cells (E7 tet⁺ KLRG1⁺) in blood at day 10 after MHC-II or control vaccination (N=6 mice per group). (E) Frequency of GL7⁺ FAS⁺ GC B cells in dLNs at day 8 post-vaccination (N=10 mice per group). Cells were pre-gated as CD19⁺ IgD⁻ live cells. (F) Frequency of plasmablasts (PB; CD19$^{int/lo}$ IgD⁻ CD138⁺ TACI⁺) at day 8 days after vaccination in dLNs (N=10 mice per group). (G-I) Mice were vaccinated on day 0 and day 3 and treated with FTY720 or NaCl vehicle at day 0, 3 and 6 after vaccination and analyzed at day 7 (N=6 mice per group). (G) Frequency of total CD4⁺ T cells in blood. (H) PADRE tet⁺ CD4⁺ T cells in dLNs. (I) Frequency of PSGL1^{lo} CXCR5⁺ and PSGL1^{hi} CXCR5⁻ PADRE tet⁺ CD4⁺ T cells in dLNs. All graphs show mean ± SD; (D-H) Unpaired Student's t-test.

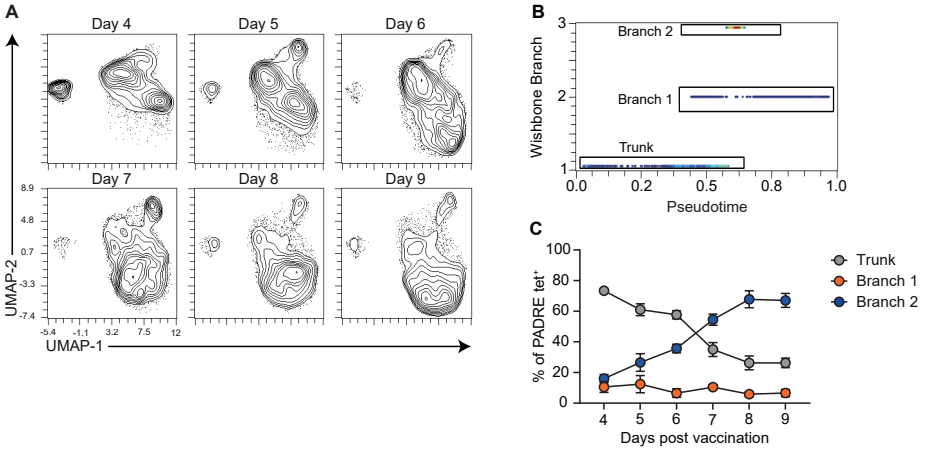

Figure S2 (related to Figure 2): Temporal analysis highlights a common differentiation branchpoint for Th1 and Tfh cells. (A) UMAP projections showing PADRE tet$^+$ CD4$^+$ T cells in the dLN of mice from day 4-9 post-vaccination (N=5 per time point). (B) Wishbone trajectory and branching of concatenated PADRE tet$^+$ CD4$^+$ T cells. (C) Frequency of PADRE tet$^+$CD4$^+$ T cells within trunk, branch 1 and branch 2 in the dLN as calculated by Wishbone. All graphs show mean ± SD.

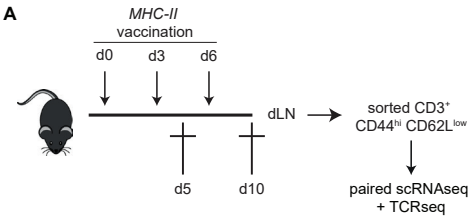

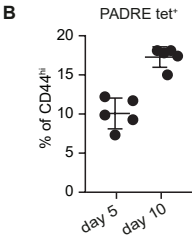

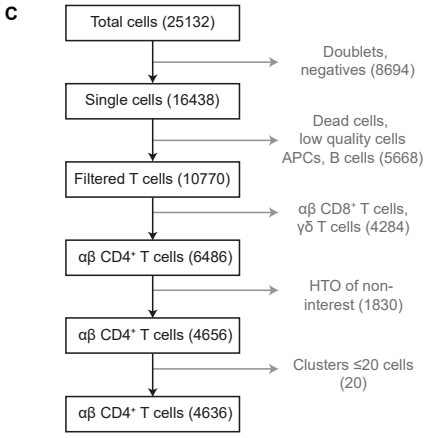

D

	Cell number per cluster		
	d5	*d10*	*total*
cl.0	721	412	1133
cl.1	182	881	1063
cl.2	258	413	671
cl.3	315	299	614
cl.4	254	259	513
cl.5	310	156	466
cl.6	176	35	176

E

	Expanded TCR clones per cluster		
	unique	*shared*	*total*
cl.0	45	37	82
cl.1	99	117	216
cl.2	22	95	117
cl.3	0	3	3
cl.4	0	20	20
cl.5	15	85	100
cl.6	0	13	13

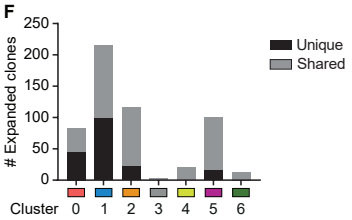

Figure S3 (related to Figure 3): scRNAseq and TCRseq of dLN-derived CD4⁺ T cells after vaccination. (A, C) Schematic overview of mouse treatment, sample preparation (A) and pipeline for quality control and filtering steps of scRNAseq data analysis (C). (B) Frequency of PADRE tet⁺ cells among CD4⁺ CD44^{hi} cells at days 5 and 10 post-vaccination (N=5 mice per timepoint). Data are representative of 2 independent experiments, graphs depict mean ± SD. (D, E) Tables report numbers of cells identified per cluster (cl.) at days 5 and 10 (D), or numbers of expanded TCR clones per cluster, which identify clones that were uniquely found in one cluster, or were shared between at least two clusters (E). (F) Number of expanded TCR clones (>1 cell per clone) per cluster. Black: TCR clones unique to one cluster; grey: TCR clones shared between two or more clusters.

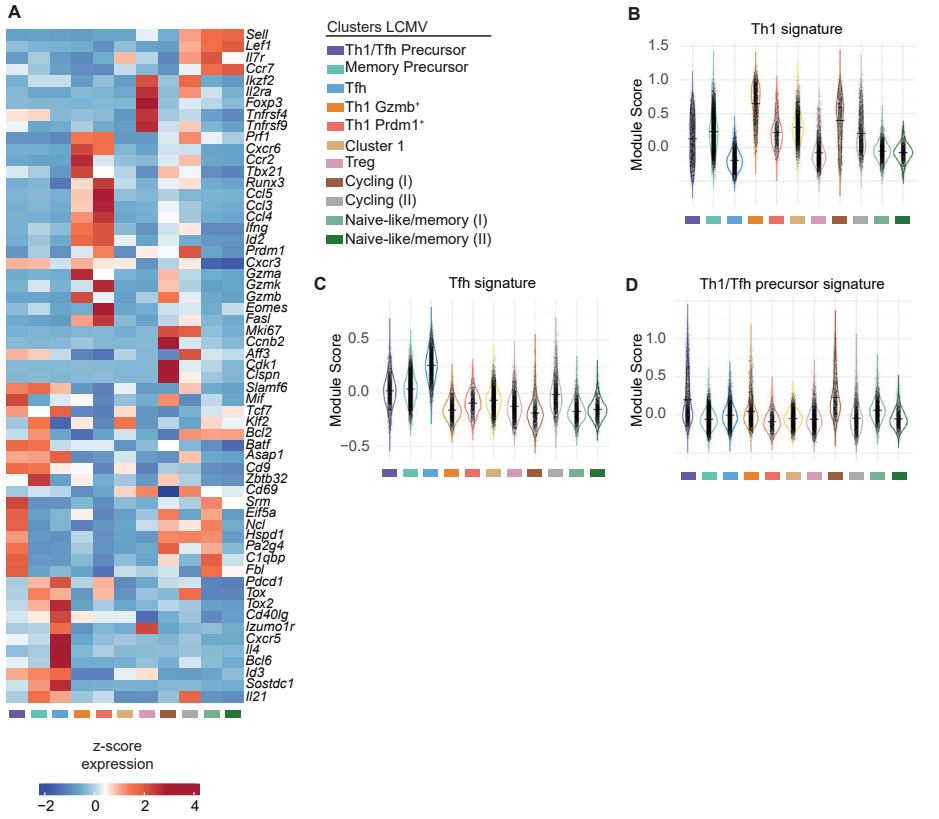

Figure S4 (related to Figure 4): Gene profile of the LCMV-specific CD4⁺ T cells. (A) Heatmap showing selected differentially expressed genes across clusters of LCMV-specific CD4⁺ T cells. Colors indicate normalized (z-scored) gene-expression levels within each cluster. (B-D) Violin plots displaying module scores for vaccine-induced Th1 (B), Tfh (C), and Th1/Tfh precursor (D) gene signatures across clusters of GP66 tet⁺ LCMV-specific CD4⁺ T cells isolated from mice infected with LCMV-Armstrong or LCMV-Clone 13 at days 8 and 21 post-infection. Module scores indicate per-cell expression levels of genes within each signature, based on normalized expression value.

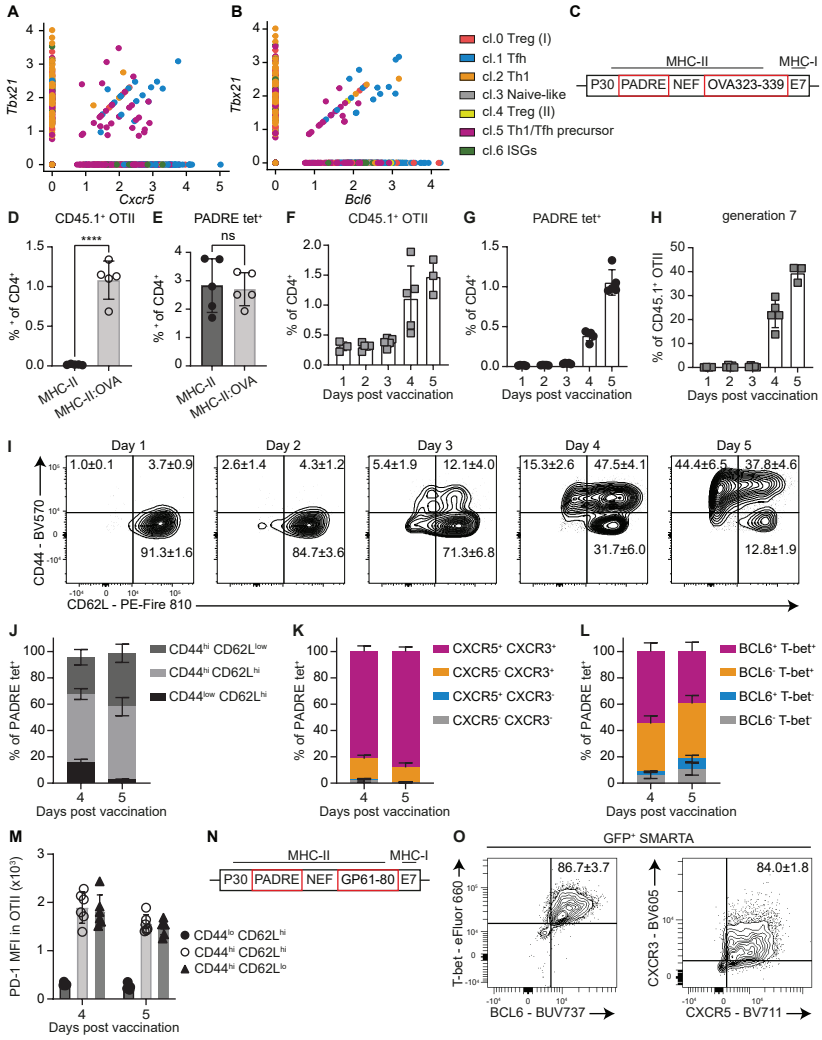

Figure S5 (related to Figure 5): Phenotypic analysis of the common Th1/Tfh precursor pool. (A-B) Expression levels per cell of Tbx21 and Cxcr5 (A) or Tbx21 and Bcl6 (B) mRNA. CD4⁺ T cell clusters from scRNAseq of vaccinated mice are color-coded as in Figure 3. (C) Schematic overview of epitopes in MHC-II:OVA vaccine. (D, E) Frequency of CD45.1⁺ OTII (D) or PADRE tet⁺ (E) CD4⁺ T cells in the dLN of mice at day 8 after vaccination with MHC-II or MHC-II:OVA plasmid (N=5 mice per group), as determined by flow cytometry. Unpaired Student's t-test. (F-M) Mice were vaccinated once with MHC-II:OVA vaccine. (F, G) Frequency of CD45.1⁺ OTII (F) or CD45.2⁺ PADRE tet⁺ (G) CD4⁺ T cells at indicated times after vaccination, as determined by flow cytometry. (H) Frequency of CD45.1⁺ OTII that underwent 7 cell divisions at indicated time points post-vaccination (N=3-5 per timepoint), as determined by CFSE dilution. I) Flow cytometric detection of CD44 and CD62L on CD45.1⁺ OTII cells in the dLN at indicated time points. (J-L) Graphs displaying mean ± SD of CD44 and CD62L (K), CXCR5 and CXCR3 (L), or BCL6 and T-bet (M) protein levels as detected by flow cytometry in PADRE tet⁺ CD4+ T cells at days 4 and 5 post-vaccination (N=5 per time point). (M) Median fluorescence intensity (MFI) for PD-1 on CD44^{lo} CD62L^{hi}, CD44^{hi} CD62L^{hi}, and CD44^{hi} CD62L^{lo} CD45.1⁺ OTII cells at days 4 or 5 after vaccination. (N) Schematic overview of epitopes in the LCMV-GP$_{61-80}$ modified MHC-II vaccine. (O) Mice were vaccinated once with MHCII:LCMV-GP$_{61-80}$ vaccine. Representative contour plots depicting T-bet and BCL6 or CXCR3 and CXCR5 protein levels in GFP⁺ SMARTA cells at day 4 post-vaccination (N=6 mice per group). All graphs show mean ± SD.

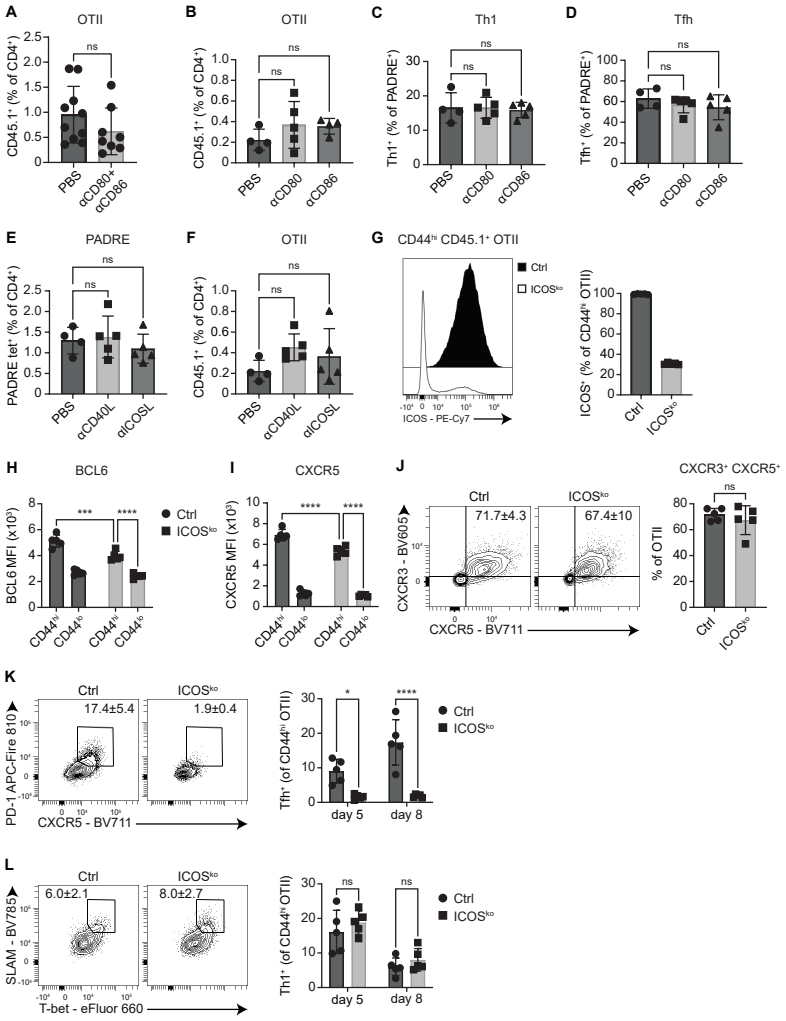

Figure S6 (related to Figure 6): Costimulatory molecules driving CD4⁺ T-cell differentiation. Mice received OTII cells and MHC-II:OVA vaccine and were treated with blocking mAbs to the indicated molecules or PBS (control). At day 5 after vaccination, dLNs were harvested and cells were analyzed by flow cytometry. (A) Mice received one vaccination. Quantification of CD45.1⁺ OTII cells in dLNs after blocking CD80 and CD86 or control (N=9-10 mice per group pooled from two experiments). (B-D) Quantification of CD45.1⁺ OTII cells (B), CD45.2⁺ PADRE tet⁺ SLAM⁺ Tbet+ Th1 cells (C) and CD45.2⁺ PADRE tet⁺CXCR5⁺ PD-1⁺ Tfh cells (D) in dLN after blocking either CD80, or CD86, or control. (E-F) Quantification of CD45.2⁺ PADRE tet⁺ (E) and CD45.1⁺ OT-II (F) cells in dLN after blocking CD40L or ICOSL, or control (N=4-5 mice per group). (G-L) Mice received OTII cells after CRISPR/Cas9-gene editing for ICOS (ICOSko) or with a non-targeting gRNA (Ctrl) . Mice were subsequently vaccinated with MHC-II:OVA, and dLNs were isolated at day 5 (G-L) or day 8 (K,L) (N=5 mice per group per timepoint). G) Concatenated histograms and frequency depicting ICOS expression (left) and the frequency of ICOS⁺ cells (right) in CD44^{hi} CD45.1⁺ OTII cells. (H-L) For the ICOSko group, only ICOS⁻ cells were assessed. (H, I) MFI of BCL6 (H) and CXCR5 (I) in activated CD44^{hi} and naive CD44^{lo} OTII cells. (J-L) Representative contour plots and graphs depicting frequency of CXCR3⁺ CXCR5⁺ Th1/Tfh precursor cells (J), CXCR5⁺ PD-1⁺ Tfh (K), and SLAM⁺ T-bet⁺ Th1 (L) CD44^{hi} OTII cells. (A, J) Unpaired Student's t-test. (B-F) One-Way ANOVA with Dunnett's post hoc test was used to correct for multiple testing when comparing inhibitory conditions to control. Data are representative of at least two independent experiments. (H, I, K, L) Two-way ANOVA with Šidák post hoc test was used. (A-L). All graphs show mean ± SD.

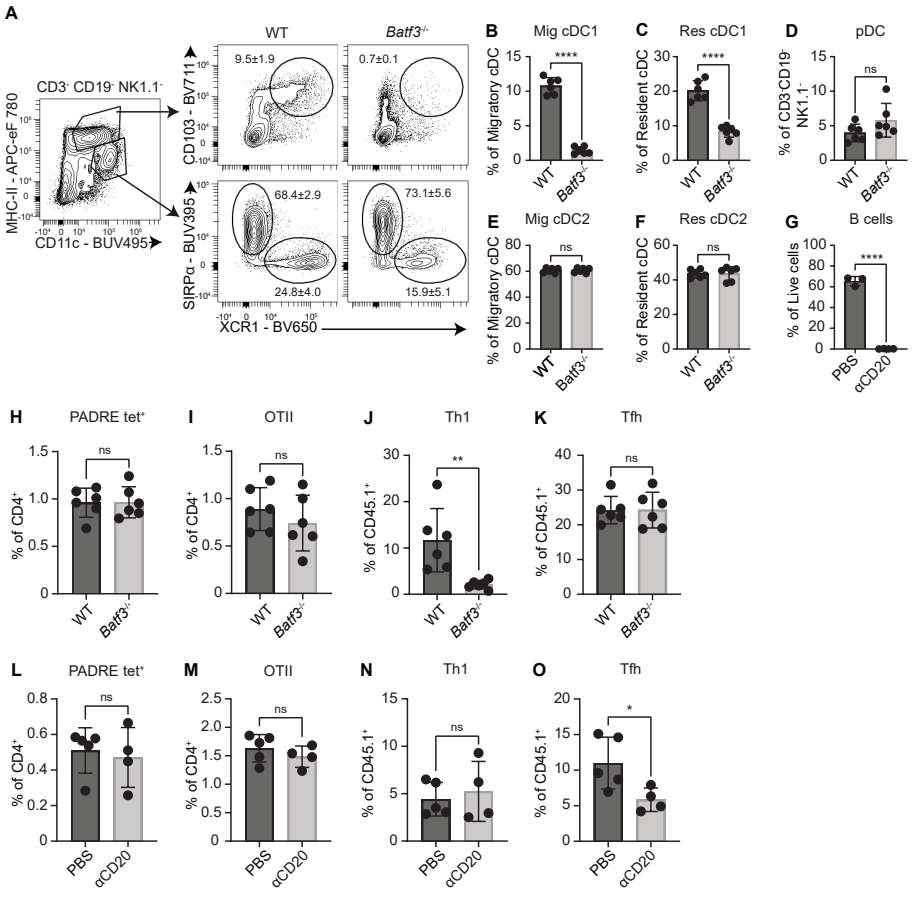

Figure S7 (related to Figure 7): Antigen presenting cells driving CD4⁺ T-cell differentiation. WT or Batf3-/- mice received OTII cells, were vaccinated once with MHC-II:OVA vaccine and were treated with depleting anti-CD20 mAb or PBS (control) as indicated. At day 5 after vaccination, dLNs were harvested and cells were analyzed by flow cytometry. (A) Gating strategy to identify migratory cDC1s (MHC-II^{hi} CD11c^{int} CD103^{+} XCR1^{+}), resident cDC1s (MHC-II^{int} CD11c^{hi} XCR1^{+}SIRPα^{-}) and resident cDC2s (MHC-II^{int} CD11c^{hi} XCR1^{-} SIRPα^{+}) in the dLN at day 3 post-vaccination. (B-F) Quantification of migratory (B) and resident (C) cDC1, pDCs (Ly6C^{+} Siglec H^{+}; D), migratory (MHC-II^{hi} CD11c^{int} XCR1^{-} SIRPα^{+}; E) and resident cDC2 (F) in WT and Batf3-/- mice (N=6 mice per group). (G) Quantification of CD19^{+} B cells in peripheral blood two days after treatment with anti-CD20 mAb (N=3-4 mice per group). (H, L) Frequency of PADRE tet^{+} among CD4^{+} T cells in dLNs of indicated test groups. (I, M) Frequency of CD45.1^{+} OTII cells in dLN of indicated test groups. (J-K, N-O) Frequency of CD45.1^{+} OTII cells with SLAM^{+} T-bet^{+} Th1 phenotype (J, N) or CXCR5^{+} PD-1^{+} Tfh phenotype (K, O) CD45.1^{+} OTII cells in dLNs of indicated test groups. All graphs depict mean ± SD (N=6 mice per group in A-K; N=4-5 mice per group in L-O). Unpaired Student's t-test.

Description of Supplementary Tables

Supplementary Table 1:

List of differentially expressed genes by $CD4^+$ T cell clusters generated by scRNAseq after DNA tattoo vaccination.

Supplementary Table 2:

List of differentially expressed genes by $CD4^+$ T cell clusters derived from Xia *et al.*, 2022 (ref. 54).

Supplementary Table 3:

List of differentially expressed genes in LCMV-specific Th1/Tfh precursor and LCMV-specific memory-precursor cell clusters derived from Xia *et al.*, 2022 (ref. 54).

Supplementary Table 4:

Gene signature of malaria-induced Th1/Tfh precursor cells derived from Lönnberg *et al.*, 2017 (ref. 4).

Supplementary Table 5:

List of differentially expressed genes between clusters 1 (Tfh) and cluster 2 (Th1) $CD4^+$ T cells identified by scRNAseq after DNA tattoo vaccination.

Supplementary Table 6:

List of differentially expressed genes between clusters 5 (Th1/Tfh precursors) and cluster 3 (naive-like) $CD4^+$ T cells identified by scRNAseq after DNA tattoo vaccination.

Key Resource Table

Details of used reagents and resources

All Supplementary Tables are available at DOI: 10.1016/j.celrep.2026.117296